Cell Stem Cell

Article

Human adult hippocampal neurogenesis is shaped by neuropsychiatric disorders, demographics, and lifestyle-related factors

Graphical abstract

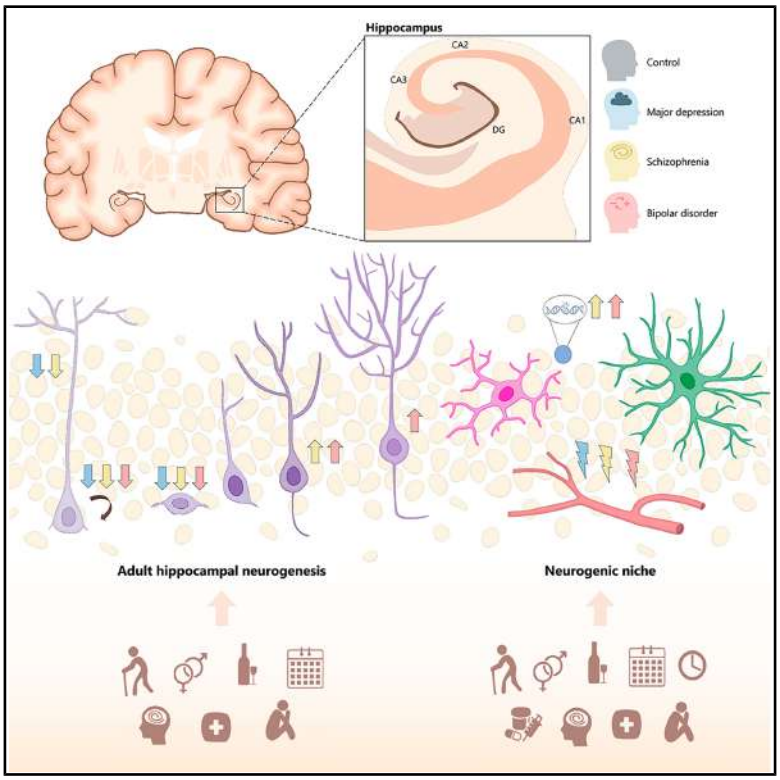

Highlights

- The proliferation of neural stem cells and neuroblasts is impaired in psychiatric disorders
- Newborn neuron maturation is differentially affected in distinct psychiatric disorders
- The homeostasis of the dentate gyrus is altered in patients with psychiatric disorders
- Demographics and lifestyle-related factors modulate human adult hippocampal neurogenesis

Authors

Berenice Márquez-Valadez, Marta Gallardo-Caballero, María Llorens-Martín

Correspondence

m.llorens@csic.es

In brief

Márquez-Valadez and colleagues show that neuropsychiatric disorders alter the generation of new neurons in the adult human brain. Major depression, schizophrenia, and bipolar disorder disrupt early stages of hippocampal neurogenesis and its supportive environment, with lifestyle factors further modulating these effects—even in healthy individuals.

Márquez-Valadez et al., 2025, Cell Stem Cell *32*, 1–18
October 2, 2025
https://doi.org/10.1016/j.stem.2025.08.010

CellPress

Cell Stem Cell

CellPress
OPEN ACCESS

Article

Human adult hippocampal neurogenesis is shaped by neuropsychiatric disorders, demographics, and lifestyle-related factors

Berenice Márquez-Valadez,[1,2,3,4] Marta Gallardo-Caballero,[1,2,3,4] and María Llorens-Martín[1,2,3,5,*]
[1]Department of Molecular Neuropathology, Centro de Biología Molecular "Severo Ochoa" (CBMSO), Spanish Research Council (CSIC)–Universidad Autónoma de Madrid (UAM), Madrid, Spain
[2]Center for Networked Biomedical Research on Neurodegenerative Diseases (CIBERNED), Madrid, Spain
[3]Department of Molecular Biology, Faculty of Sciences, Universidad Autónoma de Madrid, Madrid, Spain
[4]These authors contributed equally
[5]Lead contact
*Correspondence: m.llorens@csic.es
https://doi.org/10.1016/j.stem.2025.08.010

SUMMARY

Adult hippocampal neurogenesis (AHN) regulates hippocampal-dependent functions and is targeted by physiological aging and neurodegenerative conditions. Patients with neuropsychiatric disorders show hippocampal abnormalities that might be related to changes in AHN. Here, we sought to determine whether major depression, schizophrenia, and bipolar disorder threaten the integrity of human AHN and the homeostasis of the dentate gyrus (DG) neurogenic niche—a specialized microenvironment in which new neurons grow. Our results show that the initial and intermediate stages of AHN, as well as distinct components of the niche, are selectively affected in these disorders. Demographics and various lifestyle-related factors (such as the consumption of alcohol and drugs of abuse) modulate both AHN and the cells that compose the niche, not only in patients with these disorders but also in neurologically healthy control individuals. These data might be relevant for the design of future strategies to treat and prevent mental health conditions.

INTRODUCTION

The mammalian hippocampus generates new neurons throughout life.[1,2] New dentate granule cells (DGCs) participate in hippocampal-dependent functions by regulating learning, forgetting, and mood.[3–5] Recent single-cell RNA sequencing[6,7] and histological[8,9] studies have started to unveil human adult hippocampal neurogenesis (AHN) trajectories and show that the human dentate gyrus (DG) hosts neural stem cells (NSCs) with proliferative capacity, neuroblasts, and immature neurons at distinct stages of maturation up to at least the tenth decade of life. The occurrence of AHN is supported by a specialized microenvironment, namely the DG neurogenic niche, which is enriched in glial and vascular elements.[9,10] In this niche, microglia mediate surveillance and pruning mechanisms,[11] whereas astrocytes provide trophic support to developing neurons and neural precursors.[12] Moreover, the profuse network of microcapillaries that irrigates the subgranular zone (SGZ) modulates the response of AHN to physiological and pathological stimuli.[10]

The hippocampus is particularly vulnerable to both physiological aging and neurodegenerative diseases. Moreover, structural abnormalities in this brain region are frequently observed in individuals with psychiatric disorders, contributing to impaired cognitive performance, disturbances in emotional regulation, and diminished ability to carry out everyday tasks.[13–15] Although animal models of psychiatric conditions show AHN impairments,[3,16] their limited translational validity in capturing the full complexity of human mental disorders highlights the urgent need for studies to determine whether alterations in AHN underlie the hippocampal abnormalities observed in affected patients. To address this question, we sought to determine whether the integrity of human AHN and the DG neurogenic niche are affected in patients with major depression (MD), schizophrenia (SCH), and bipolar disorder (BD). Our analysis used high-quality post-mortem hippocampal samples from the well-characterized neuropathology consortium provided by the Stanley Medical Research Institute (SMRI), including 14 neurologically healthy control subjects and 15 individuals per diagnostic group. Samples were processed under rigorously standardized conditions and quantified through unbiased stereological methods.

Given that AHN in animal models is modulated by both intrinsic and extrinsic cues, we further explored how human AHN and key components of the DG neurogenic niche vary according to demographic variables and lifestyle-related factors. This integrative framework—combining diagnostic status, demographic and behavioral parameters, and cell-type-specific neurogenic profiling—aims to deepen our understanding of the multifactorial regulation of human AHN. In light of the scarcity of high-quality

Please cite this article in press as: Márquez-Valadez et al., Human adult hippocampal neurogenesis is shaped by neuropsychiatric disorders, demographics, and lifestyle-related factors, Cell Stem Cell (2025), https://doi.org/10.1016/j.stem.2025.08.010

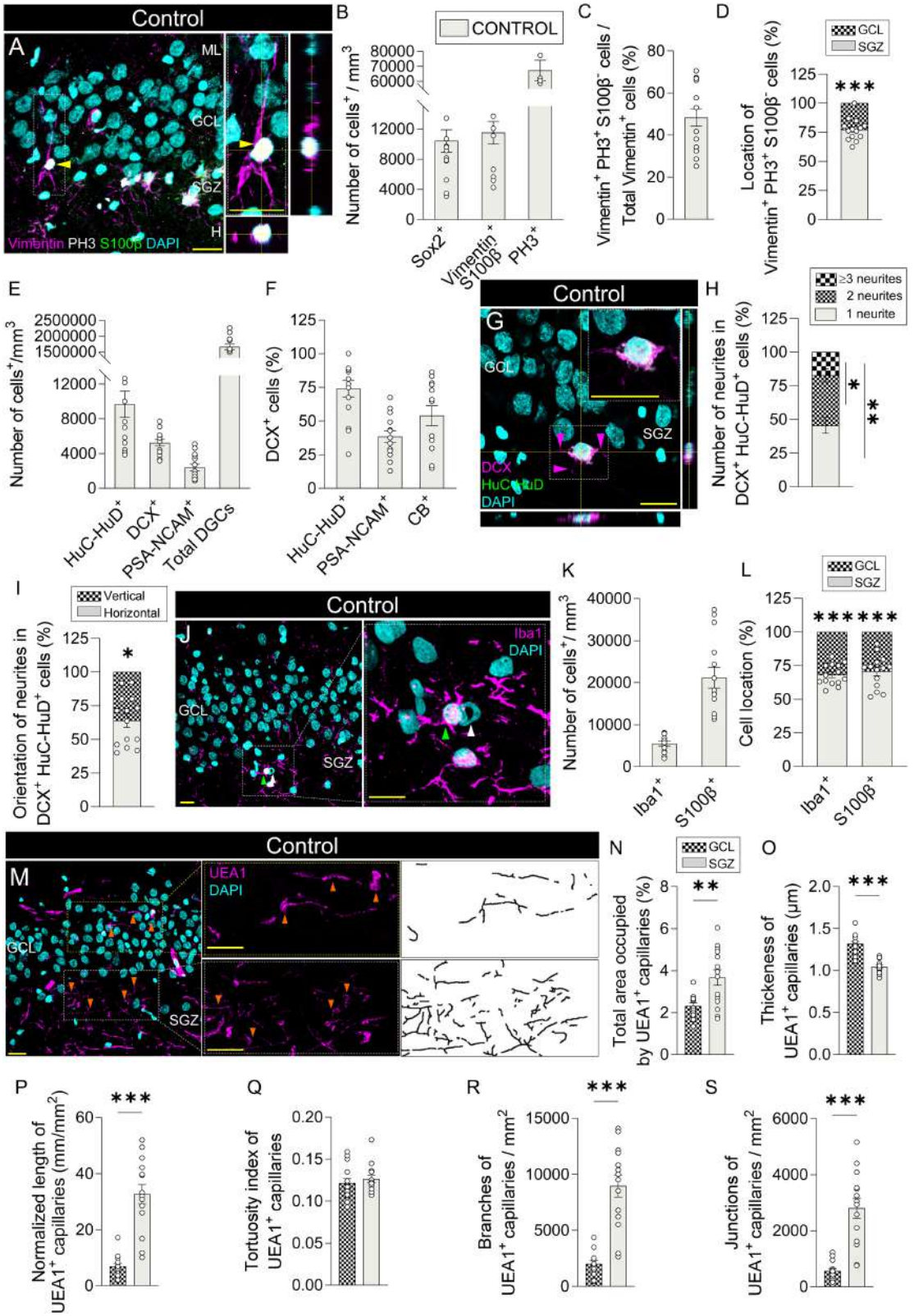

(legend on next page)

Please cite this article in press as: Márquez-Valadez et al., Human adult hippocampal neurogenesis is shaped by neuropsychiatric disorders, demographics, and lifestyle-related factors, Cell Stem Cell (2025), https://doi.org/10.1016/j.stem.2025.08.010

human tissue and the translational limitations of preclinical models, our study offers crucial insights into AHN biology in health and disease, laying the groundwork for more precise therapeutic interventions to restore neuroplasticity in neuropsychiatric disorders.

RESULTS

AHN in neurologically healthy control subjects

We first examined a cohort of 14 neurologically healthy middle-aged adult control subjects (Figures 1, 2, S1, and S2). In line with previous observations,[9,17] we detected a population of cells that expressed NSC markers, such as SRY (sex-determining region Y)-box 2 (Sox2) and vimentin, but lacked expression of S100 calcium-binding protein B (S100β), a mature astrocyte marker, thereby confirming their NSC phenotype (Figures 1A and 1B).[18] Moreover, ~48% of vimentin$^+$ cells expressed the proliferation marker phospho-histone 3 (PH3) while lacking S100β expression (Figures 1A and 1C). The remaining (PH3$^-$) NSCs may be considered presumably quiescent, thereby supporting the notion of preserved AHN throughout life.[19] These data are the first to histologically identify a population of NSCs with *in vivo* proliferative capacity in the adult human DG. In light of the age-associated increase in NSC quiescence during physiological aging,[19,20] the inclusion of middle-aged control subjects (~45 years) likely enhanced the detection sensitivity for the identified cluster of proliferative NSCs, which had eluded previous histological characterization. Moreover, the use of unfixed fresh-frozen brain samples, thin[21] glass-slide-mounted sections, a short 10-min fixation protocol, thorough tissue permeabilization, and an anti-vimentin antibody that is highly reactive against the human epitope (Figure S2 and key resources table) facilitated the detection of proliferative NSCs relative to previous studies. Likewise, identifying these proliferative NSCs at the transcriptomic level required the application of refined single-nucleus RNA sequencing and machine-learning approaches.[7] An example of an NSC with a long vertical process is shown in Figure 1A. These cells were predominantly located at the SGZ (Figure 1D). This region corresponds to the hilar border of the granule cell layer (GCL) and it forms the DG proliferative niche.[22] During AHN, dividing NSCs give rise to proliferating neuroblasts, which express doublecortin (DCX) and HuC-HuD[9] (Figures 1E–1G) and constitute the majority of proliferating cells in the human DG.[9] DCX$^+$ HuC-HuD$^+$ neuroblasts showed an immature morphology with elongated nuclei and horizontal neurites (Figures 1G–1I). Upon commitment to the neuronal lineage, immature DGCs first expressed polysialylated-neural cell adhesion molecule (PSA-NCAM) and, subsequently, calbindin (CB) (Figures 1E and 1F), while showing a single, vertically oriented, primary apical dendrite.[8,9]

AHN is orchestrated by complex crosstalk established between the microglia, astrocytes, and blood vessels/capillaries that make up the SGZ neurogenic niche[9,10] (Figures 1J–1S). Compared with the GCL, the SGZ was particularly enriched in Iba1$^+$ microglia and S100β$^+$ astrocytes (Figures 1J–1L), as well as *Ulex Europaeus* Agglutinin-I (UEA1)$^+$ capillaries (Figures 1M–1S). As in the mouse hippocampus,[10] the human SGZ vasculature shows distinctive characteristics. In particular, SGZ UEA1$^+$ capillaries were thinner (Figure 1O), longer (Figure 1P), equally tortuous (Figure 1Q), and had more branches (Figure 1R) and junctions (Figure 1S) than those of the GCL. Taken together, our data reveal that the human SGZ is markedly enriched in glial and complex vascular elements, two classical hallmarks of neurogenic niches,[23] thereby strongly supporting the potential of this region to facilitate the generation of new neurons throughout life.

We next explored the impact of demographics and alcohol consumption on AHN and the DG neurogenic niche in control individuals. We observed a decline in the area of the SGZ occupied by UEA1$^+$ capillaries, as well as in the length and the number of branches and junctions of total UEA1$^+$ capillaries (Figures 2A–2G) with age. This observation is consistent with the decreased vascularization and angiogenesis reported during aging,[23,24] as well as with histopathological evidence indicating that anatomical alterations in small vessels contribute to age-associated reductions in cerebral blood flow and subsequent cellular degeneration.[25] Together with impaired microglial phagocytic capacity,[9] the reduction in SGZ vascularization and capillary complexity indicate that halted neurogenic niche functioning may underlie age-driven AHN decline in humans.[8,26] Given that the DG is a major target of gonadal hormone signaling,[27] we assessed the impact of biological sex on the parameters analyzed.

Figure 1. AHN and DG neurogenic niche in neurologically healthy control subjects

(A) Vimentin$^+$ phospho-histone 3 (PH3)$^+$ S100 calcium-binding protein B (S100β)$^-$ proliferative neural stem cell (NSC).
(B) Density of SRY (sex-determining region Y)-box 2 (Sox2)$^+$, vimentin$^+$ S100β$^-$, and PH3$^+$ cells.
(C) Percentage of vimentin$^+$ cells that express PH3 but lack S100β expression out of the total number of vimentin$^+$ cells.
(D) Positioning of vimentin$^+$ PH3$^+$ S100β$^-$ cells.
(E) Density of HuC-HuD$^+$, doublecortin (DCX)$^+$, polysialylated-neural cell adhesion molecule (PSA-NCAM)$^+$, and total dentate granule cells (DGCs).
(F) Percentage of DCX$^+$ immature DGCs that express Huc-HuD, PSA-NCAM, and calbindin (CB).
(G) Morphology of a DCX$^+$ HuC-HuD$^+$ neuroblast.
(H and I) Number (H) and orientation (I) of neurites in DCX$^+$ HuC-HuD$^+$ neuroblasts.
(J) Iba1 staining.
(K and L) Density (K) and positioning (L) of Iba1$^+$ microglia and S100β$^+$ astrocytes.
(M) Vascularization of the human DG and digitalization of *Ulex Europaeus* Agglutinin-I (UEA1)$^+$ vascular skeleton in Fiji.
(N) Total area occupied by UEA1$^+$ capillaries in the granule cell layer (GCL) and subgranular zone (SGZ).
(O–S) Thickness (O), normalized length (P), tortuosity index (Q), and number of branches (R) and junctions (S) of UEA1$^+$ capillaries.
n = 14 neurologically healthy control subjects.
Graphs represent mean values ± SEM. ML, molecular layer; H, hilus. Yellow scale bar: 20 μm. Yellow triangle: proliferative NSC. Magenta triangles: neurites. Green triangle: microglia. White triangle: pycnotic nucleus. Orange triangles: capillaries.
**$0.01 > p \geq 0.001$; ***$p < 0.001$.
Detailed results of statistical comparisons are shown in Data S1.

Please cite this article in press as: Márquez-Valadez et al., Human adult hippocampal neurogenesis is shaped by neuropsychiatric disorders, demographics, and lifestyle-related factors, Cell Stem Cell (2025), https://doi.org/10.1016/j.stem.2025.08.010

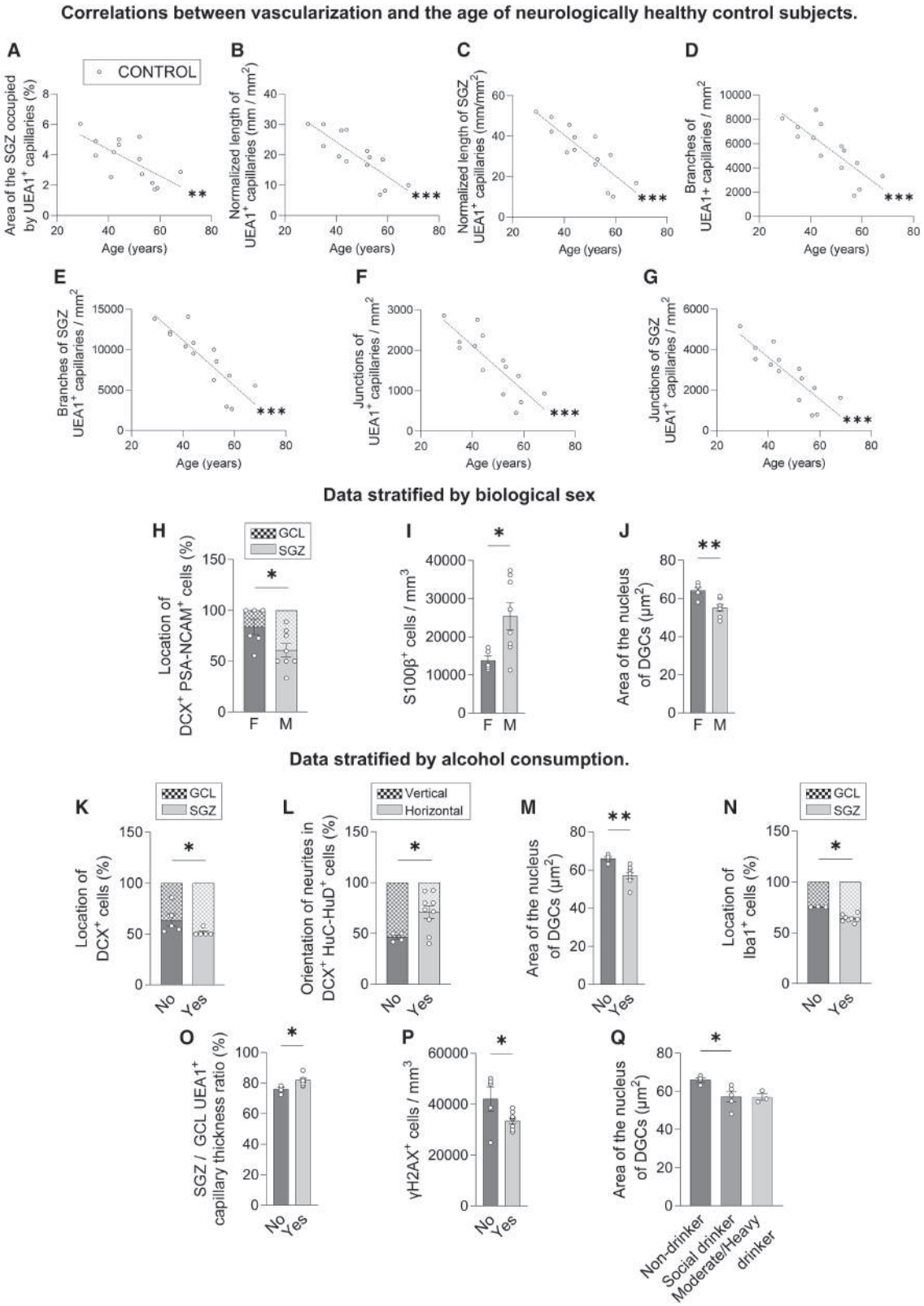

(legend on next page)

Female subjects showed a reduction in the percentages of immature DGCs in the GCL (Figure 2H) but an increase in the area of DGC nuclei (Figure 2J). We also observed a decreased density of S100β$^+$ astrocytes in females compared with males (Figure 2I). This finding aligns with previous reports describing reduced astrocytic glucocorticoid receptor expression[28] and sex-dependent alteration of transcriptional profiles.[29] Alcohol consumption altered the positioning and morphology of immature DGCs and neuroblasts (Figures 2K and 2L), reduced the nuclear area of DGCs (Figures 2M and 2Q), increased Iba1$^+$ GCL microglia (Figure 2N) and the SGZ/GCL capillary thickness ratio (Figure 2O), and reduced the density of cells positive for phosphorylated H2AX (γH2AX), a marker of DNA damage/repair[30] (Figure 2P). These results point to an altered DG microenvironment in alcohol consumers. To further study the potential dose-dependent effects of alcohol consumption, we performed an analysis based on daily alcohol intake categories (see STAR Methods section). In this context, although previous studies have reported reductions in the number of NSCs[31] in individuals with high levels of alcohol consumption, as well as in mature[32] and immature[31] DGCs, our results did not reveal additive effects of high-dose alcohol exposure on AHN in neurologically healthy controls.

Our data show the presence of proliferative NSCs and neuroblasts, and also immature neurons at distinct differentiation stages, in the adult human DG and reveal the modulation of AHN and the cellular composition of the DG neurogenic niche by demographic factors and alcohol consumption in healthy adults.

AHN in patients with MD

MD, which is characterized by persistent low mood, sadness, despair, and anhedonia, is one of the primary causes of disease burden and disability worldwide. Patients with MD show diverse hippocampal structural abnormalities,[13] including volume reductions.[33] Given the pro-neurogenic effect of antidepressants in mice,[34] impaired AHN has been proposed to underlie the aforementioned alterations.[35] Previous studies report unchanged[36] or decreased proliferation in MD patients,[37,38] although the phenotype of proliferating cells was not addressed. To tackle this question, here we sought to determine whether the entire AHN trajectory and the integrity of the DG neurogenic niche were altered in patients with this disorder (Figures 3, 4, S1, and S3–S5). Our results revealed decreased cell proliferation (Figure 3B). These changes were not attributed to S100β$^+$ astrocytes or vimentin$^-$ S100β$^-$ cells (Figures 3D and S3D). Conversely, the density (Figures 3A and 3B) and proliferative capacity of vimentin$^+$ S100B$^-$ NSCs were reduced, as shown by the decreased percentage and density of vimentin$^+$ S100B$^-$ NSCs expressing PH3 (Figures 3C–3E). Moreover, the diminished density of HuC-HuD$^+$ cells (Figures 3F and 3G) and the percentage of DCX$^+$ cells expressing HuC-HuD (Figure 3H) also pointed to reduced neuroblast proliferation in these patients. Conversely, unchanged densities of mature DGCs and DCX$^+$ and PSA-NCAM$^+$ immature DGCs (Figure 3F) were observed. Neither the percentages of the subpopulations of the latter (Figure 3H), their morphology/positioning (Figures 3I–3K, S3I–S3K, S3P, and S3Q), nor the ratios reflecting early differentiation/proliferation (Figure S3B) and late/early differentiation (Figure S3C) were altered, thereby suggesting a selective impact of MD on the initial stages of AHN. Negative correlations between age and the density of proliferative NSCs (Figures 4A and S5A) and immature DGCs (Figure 4B) were detected in these patients. Female subjects presented further decreased densities (Figure 4C) and percentages (Figure 4E) of differentiated DGCs but showed an increased proportion of immature counterparts (Figure 4D). Similarly, the higher proportion of horizontal neurites in DCX$^+$ cells (Figure 4F) points to impaired DGC maturation in female patients. In this regard, previous studies have reported either sex-dependent effects[39,40] or no significant influence[37,38,41] of biological sex on AHN in patients with MD. However, female subjects show a higher prevalence of MD and an increased odds ratio for antidepressant treatment resistance relative to their male counterparts.[42] In addition, alcohol consumption increased the percentage of SGZ neuroblasts (Figure 4H) and immature DGCs (Figure 4I). These alterations in positioning were aggravated in a dose-dependent manner (Figures 4J and 4K).

We observed unchanged densities of microglia and astrocytes in patients with MD (Figures 3L and 3M), a finding that is in line with previous studies.[41,43] However, we observed increased tortuosity of both total and SGZ UEA1$^+$ capillaries (Figures 3N, 3O, and S4), indicating alterations in the geometric organization of the vasculature network and potentially affecting microcirculatory efficiency and tissue perfusion.[44] Notably, several authors have proposed that cerebrovascular dysfunction is a contributing factor to the pathophysiology of MD.[45] Accordingly, we observed that vascular changes correlated positively with disease duration (Figures S5B–S5D), while both vascular and microglial alterations showed negative correlations with the age at disease onset (Figures S5E and S5F). A higher percentage of astrocytes (Figure 4G) and decreased vascularization (Figure S5H) were detected in the SGZ of females, and increased capillary tortuosity in the GCL (Figure S5I) was observed in

Figure 2. Statistically significant comparisons of data obtained from neurologically healthy control subjects

(A–G) Statistically significant correlations between the age of the subject and area of the subgranular zone (SGZ) occupied by *Ulex Europaeus* Agglutinin-I (UEA1)$^+$ capillaries (%) (A), normalized length of total (granule cell layer [GCL] + SGZ) (B), and SGZ (C) UEA1$^+$ capillaries, total (D) and SGZ (E) number of branches of UEA1$^+$ capillaries, and total (F) and SGZ (G) number of junctions of UEA1$^+$ capillaries.

(H–Q) Statistically significant comparisons of data obtained from healthy control subjects stratified by biological sex (H)–(J) and alcohol consumption (K)–(Q). (H) Location of doublecortin (DCX)$^+$, polysialylated-neural cell adhesion molecule (PSA-NCAM)$^+$, and immature dentate granule cells (DGCs). (I) Density of S100 calcium-binding protein B (S100β)$^+$ astrocytes. (J) Area of the nucleus of DGCs. (K) Location of DCX$^+$ immature DGCs. (L) Neurite orientation of DCX$^+$ HuC-HuD$^+$ neuroblasts. (M) Area of the nucleus of DGCs. (N) Location of Iba1$^+$ microglia. (O) SGZ/GCL capillary thickness ratio. (P) Density of phosphorylated H2AX (γH2AX)$^+$ cells. (Q) Area of the nucleus of DGCs.

F, female; M, male. n = 14 neurologically healthy control subjects. Graphs represent mean values ± SEM.

*$0.05 > p \geq 0.01$; **$0.01 > p \geq 0.001$; and ***$p < 0.001$.

Detailed results of statistical comparisons are shown in Data S1.

Please cite this article in press as: Márquez-Valadez et al., Human adult hippocampal neurogenesis is shaped by neuropsychiatric disorders, demographics, and lifestyle-related factors, Cell Stem Cell (2025), https://doi.org/10.1016/j.stem.2025.08.010

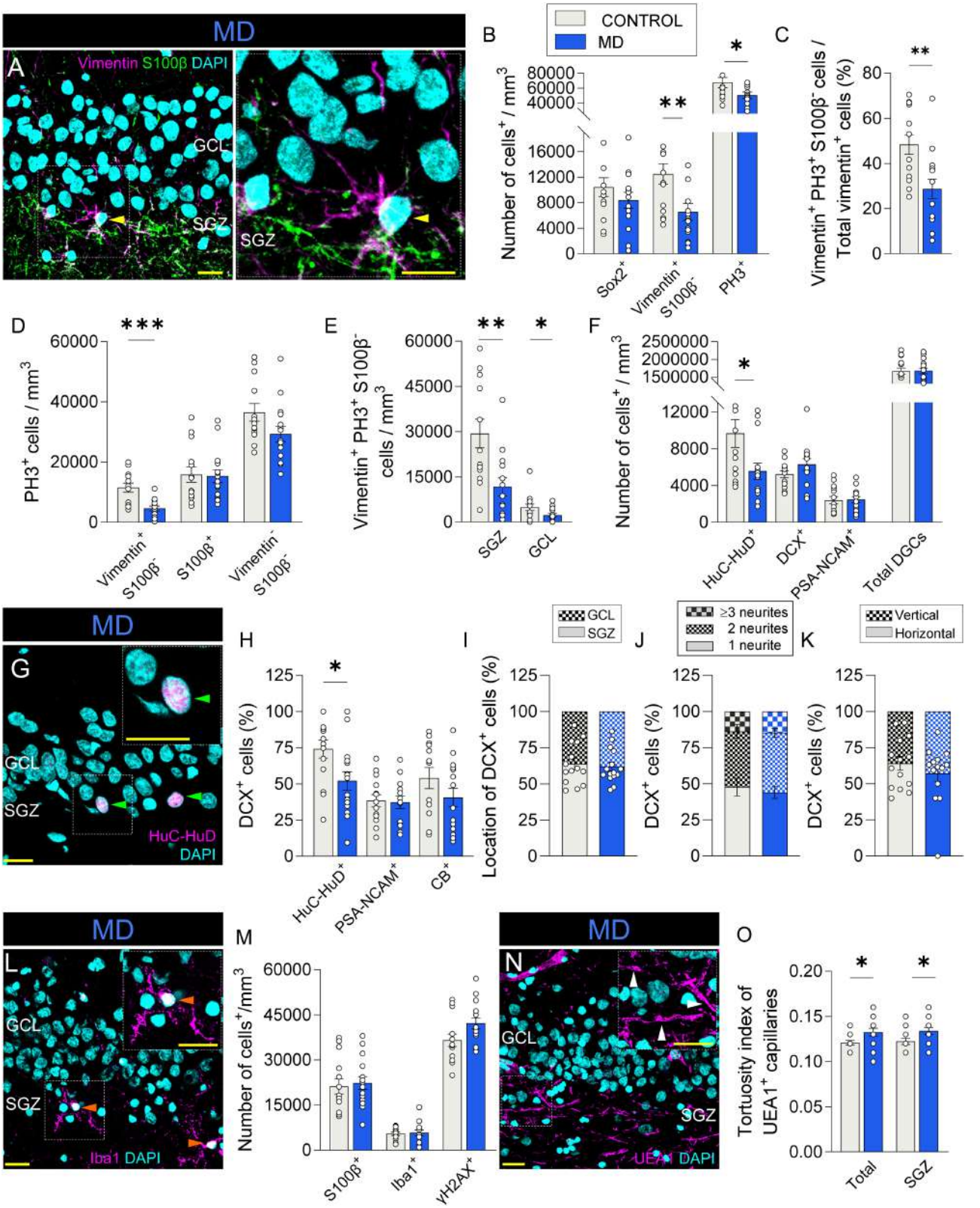

(legend on next page)

Please cite this article in press as: Márquez-Valadez et al., Human adult hippocampal neurogenesis is shaped by neuropsychiatric disorders, demographics, and lifestyle-related factors, Cell Stem Cell (2025), https://doi.org/10.1016/j.stem.2025.08.010

subjects who committed suicide. The consumption of high doses of alcohol increased the density of Iba1$^+$ microglia (Figure S5M), altered the location of γH2AX$^+$ cells (Figure S5N), and further aggravated vascular alterations (Figure S5O).

These data indicate that the early phases of ANH—NSC and neuroblast proliferation in particular—as well as the vasculature are predominantly affected in MD. These changes were further exacerbated by age, female sex, early disease onset, high alcohol intake, and suicide. Notably, female patients and subjects consuming alcohol also showed impaired DGC differentiation.

AHN in patients with SCH

Patients with SCH present positive (psychotic), negative, and cognitive symptoms. They experience hippocampal-dependent memory impairments, which are linked to reduced hippocampal activity[46] and volume,[47,48] whereas positive symptoms are attributed to hippocampal hyper-activation.[49] Despite unchanged total cell numbers,[50] patients with SCH were reported to show reduced hippocampal proliferation.[36,51] To shed further light on these alterations, we sought to thoroughly examine each AHN stage and the components of the neurogenic niche in patients with this disorder (Figures 5, S1, and S6–S8). They showed reduced densities of vimentin$^+$ S100β′ (Figure 5C), PH3$^+$ (Figures 5A–5C), and vimentin$^+$ PH3$^+$ S100β′ cells (Figures 5E and 5F), thereby pointing to a reduced density and impaired proliferation capacity of NSCs. It should be noted that, like patients with MD, those with SCH showed no changes in the proliferation of S100β$^+$ astrocytes (Figures 5E and S6D). Conversely, the density of vimentin′ S100β′ cells is decreased in patients with SCH (Figure 5E). Moreover, the lower density of HuC-HuD$^+$ proliferative neuroblasts (Figures 5G and 5H) and reduced percentage (Figure 5I) and density (Figure S6A) of DCX$^+$ cells expressing HuC-HuD also suggest impaired neuroblast proliferation. The higher densities of DCX$^+$ and PSA-NCAM$^+$ immature DGCs (Figure 5G) were paralleled by an increase in the early differentiation/proliferation ratio (Figure S6B). These alterations occurred in the absence of positioning and morphological alterations (Figures 5J–5L, S6J, and S6K), together with an unchanged ratio of late/early differentiation of DCX$^+$ cells (Figure S6C). Taken together, these results point to increased early cell survival or lengthening of the early differentiation phases of immature DGCs in SCH. No correlations between patient age and AHN impairments were observed. Female patients showed decreased densities of DCX$^+$ cells in the GCL (Figure 5R), as well as a higher percentage of proliferative neuroblasts in the GCL (Figure 5S), whereas the morphology of these cells was altered in subjects who had committed suicide (Figures S8U and S8V). Alcohol consumption was related to an increased density of differentiated immature DGCs (Figure 5T). Patients who received a lifetime dose of anti-psychotics >5,000 mg showed a reduced density of DGCs (Figure S8AB) and altered positioning of proliferating cells (Figure S8AC) but an increased density of NSCs (Figure S8AD).

The density of Iba1$^+$ microglia and S100β$^+$ astrocytes remained unchanged (Figure 5N). However, the increased density of cells positive for γH2AX (Figures 5M and 5N) might reflect heightened reactivity of the niche in patients with SCH. A growing body of evidence supports a significant contribution of microvascular abnormalities and altered angiogenesis to the pathogenesis of SCH.[52–55] Consistent with these findings, we detected subtle vascular alterations in the DG (Figures 5O, 5P, and S7), which became more pronounced with advancing age (Figures 5Q and S8A–S8G) and correlated with disease duration (Figures S8H–S8S). Conversely, subjects who committed suicide presented attenuated vascularization alterations (Figures S8W–S8AA). Consumption of high doses of alcohol was associated with a reduced proportion of Iba1$^+$ microglia located within the SGZ (Figure S8AE).

These results point to impaired proliferation of NSCs and neuroblasts in patients with SCH. These changes were paralleled by increased densities of immature neurons at early differentiation stages and enhanced DG reactivity. In general terms, advanced age, early onset, and longer duration of the disease aggravated vascular impairments. In addition, female patients and subjects who committed suicide or consumed alcohol also presented impaired immature neuron differentiation and alterations in microglia and the vasculature. Treatment with anti-psychotics normalized NSC densities.

AHN in patients with BD

BD is a mental health condition that causes unpredictable changes in mood and behavior, which range from mania to depression, resulting in significant distress and difficulty in all

Figure 3. AHN and DG neurogenic niche in patients with MD

(A) Vimentin$^+$ S100 calcium-binding protein B (S100β)′ neural stem cell (NSC).
(B) Density of SRY (sex-determining region Y)-box 2 (Sox2)$^+$, vimentin$^+$ S100β′ , and phospho-histone 3 (PH3)$^+$ cells.
(C) Percentage of vimentin$^+$ cells that express PH3 but lack S100β expression out of the total number of vimentin$^+$ cells.
(D) Density of distinct subpopulations of PH3$^+$ cells.
(E) Density of vimentin$^+$ PH3$^+$ S100β′ in the granule cell layer (GCL) and the subgranular zone (SGZ).
(F) Density of HuC-HuD$^+$, doublecortin (DCX)$^+$, polysialylated-neural cell adhesion molecule (PSA-NCAM)$^+$, and total dentate granule cells (DGCs).
(G) HuC-HuD$^+$ proliferative neuroblasts.
(H) Percentage of DCX$^+$ immature DGCs that express Huc-HuD, PSA-NCAM, and calbindin (CB).
(I–K) Cell location (I) and number (J) and orientation (K) of neurites of DCX$^+$ cells.
(L) Iba1 staining.
(M) Density of S100β$^+$, Iba1$^+$, and phosphorylated H2AX (γH2AX)$^+$ cells.
(N) Vascularization of the DG.
(O) Tortuosity index of total (GCL + SGZ) and SGZ *Ulex Europaeus* Agglutinin-I (UEA1)$^+$ capillaries.
n = 14 neurologically healthy control subjects and 15 patients with MD. Graphs represent mean values ± SEM. Yellow scale bar: 20 μm. Yellow triangle: NSC. Green triangles: HuC-HuD$^+$ neuroblasts. Orange triangles: microglia. White triangles: capillaries.
*$0.05 > p \geq 0.01$; **$0.01 > p \geq 0.001$; ***$p < 0.001$.
Detailed results of statistical comparisons are shown in Data S1.

Please cite this article in press as: Márquez-Valadez et al., Human adult hippocampal neurogenesis is shaped by neuropsychiatric disorders, demographics, and lifestyle-related factors, Cell Stem Cell (2025), https://doi.org/10.1016/j.stem.2025.08.010

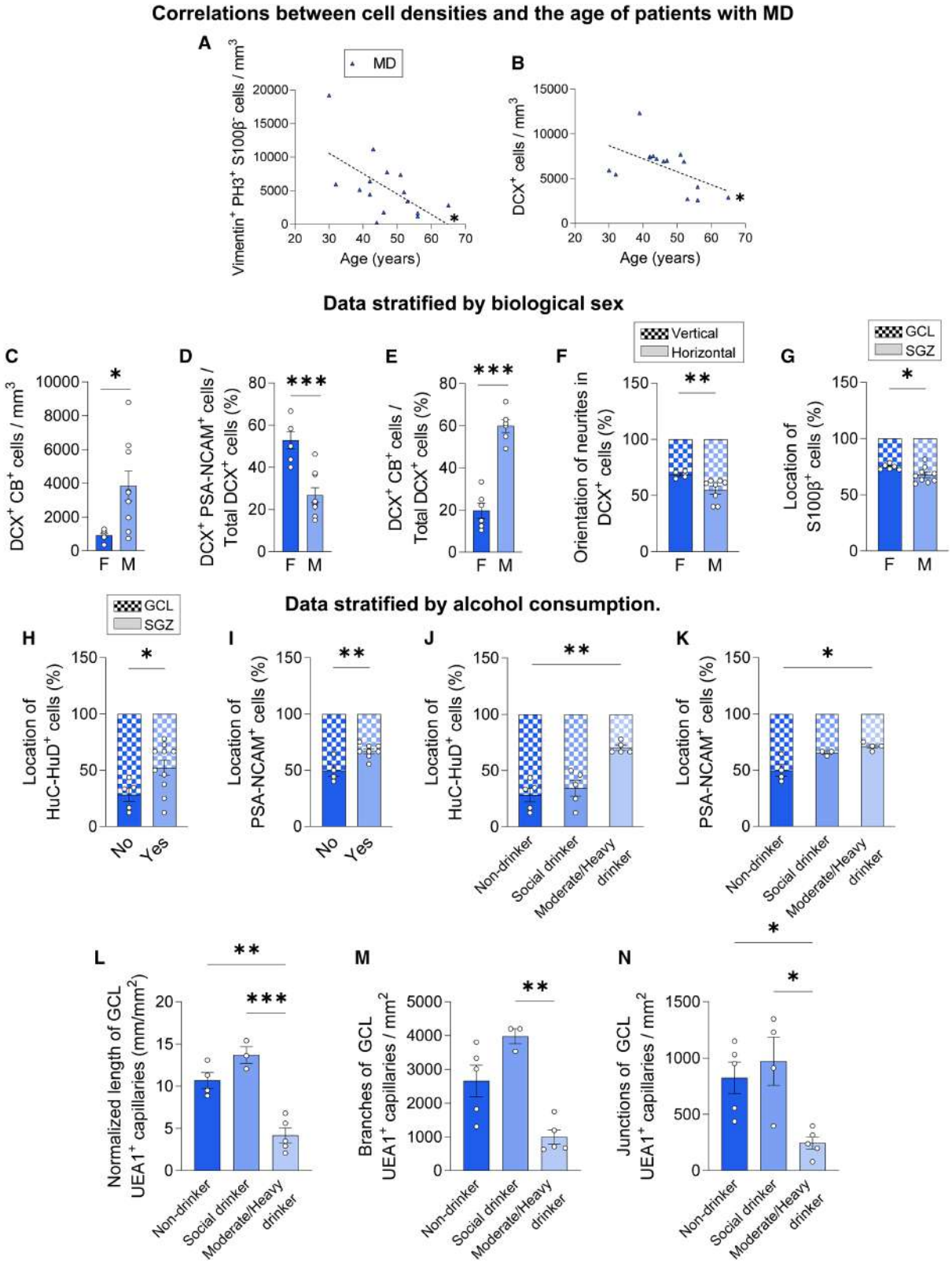

Figure 4. Statistically significant comparisons of data obtained from patients with MD

(A and B) Statistically significant correlations between the age of the subject and the density of vimentin$^+$ phospho-histone 3 (PH3)$^+$ S100 calcium-binding protein B (S100β)′ proliferative neural stem cells (NSCs) (A) and doublecortin (DCX)$^+$ immature dentate granule cells (DGCs) (B).

(legend continued on next page)

aspects of life. Despite differing diagnostic clinical criteria, SCH and BD present overlapping symptoms, including cognitive impairments putatively linked to hippocampal dysfunction.[56] In BD patients, increased hippocampal volume may be related to changes in AHN.[14] However, solid evidence supporting this affirmation remains elusive. To address this question, we sought to determine whether AHN and the DG neurogenic niche were affected in BD (Figures 6, S1, and S9–S12). Despite the unchanged density of NSCs (Figures 6A–6C), the reduced percentage of the latter expressing PH3 (Figure 6D), and the decrease in the density of SGZ vimentin$^+$ S100β$'$ PH3$^+$ proliferative NSCs (Figure 6F), pointed to increased NSC quiescence. Proliferative changes were not related to the proliferation of S100β$^+$ astrocytes or that of vimentin$'$ S100β$'$ cells (Figure 6E). Conversely, the percentage of DCX$^+$ cells that express HuC-HuD was reduced (Figure 6I), whereas the density of immature DGCs at early and late differentiation stages was increased (Figures 6G, 6H, and S9A). No changes in their positioning or morphology (Figures 6J–6L, S9J, and S9K), or in the ratios indicating early differentiation/proliferation (Figure S9B) and late/early differentiation (Figure S9C) of these cells, were detected. These data suggest generalized increases in DCX$^+$ immature DGC survival paralleled by reduced proliferation. Female subjects showed increased percentages of Sox2$^+$ cells in the SGZ (Figure 6R) and a decreased density of immature DGCs (Figure 6S). A negative correlation between the density of immature DGCs in the SGZ and age was observed (Figure S11A). Patients who received lifetime doses of anti-psychotics >5,000 mg presented an increased percentage of immature DGCs in the SGZ (Figure S12O). Subjects who committed suicide showed an increased density and percentage of proliferative neuroblasts (Figures S12G and S12H) and an increased percentage of immature DGCs in the GCL (Figures S12I and S12J). In patients with psychosis, more immature DGCs at early differentiation stages were present (Figure S12K). Higher levels of alcohol consumption (i.e., moderate to heavy drinking) were associated with altered percentages and spatial distribution of multiple cellular subpopulations compared with social drinkers (Figures S12W–S12AA).

Despite unchanged densities of Iba1$^+$ microglia and S100β$^+$ astrocytes, higher densities of γH2AX$^+$ cells (Figures 6M and 6N) point to disrupted DG homeostasis. In line with the increased vascular morbidity,[57] hypoperfusion in BD mood episodes, and hypoactive cerebral blood flow responses to emotional or cognitive challenges[58] found in patients with BD, we also observed altered vascularization in the DG (Figures 6O, 6P, and S10). Some of the vascular and glial impairments negatively correlated with patient age (Figures 6Q and S11C) and disease onset (Figure S11I) but positively correlated with disease duration (Figures S11D–S11H). Female sex (Figures 6T–6V and S12B–S12F), psychosis (Figure S12L), and consumption of drugs of abuse (Figures S12M and S12N) also resulted in further glial and vascular alterations. Treatment with anti-psychotics resulted in increased vascularization (Figures S12P–S12V).

These data reveal impaired NSC and neuroblast proliferation, increased densities of immature DGCs at early and late maturation stages, and alterations in the components of the DG neurogenic niche in patients with BD. Sex-driven AHN alterations were detected. Advanced age and early onset and longer duration of the disease, as well as high alcohol consumption, psychotic episodes, or death by suicide, exacerbated some of the aforementioned alterations in BD.

DISCUSSION

AHN is a lifelong form of neural plasticity regulated by numerous intrinsic and extrinsic factors and is impaired in patients with neurodegenerative diseases.[9] Growing evidence highlights a complex interplay between neurodegenerative and psychiatric disorders, particularly given their overlapping clinical and biological features. For instance, Alzheimer's disease (AD) and MD share several neuropathological hallmarks, including the dysregulation of the hypothalamic-pituitary-adrenal axis, hippocampal atrophy, and chronic neuroinflammation, all of which may contribute to AHN impairments.[59,60] Moreover, studies in mice have shown that depressive-like behaviors precede amyloid-β plaque deposition, raising the possibility that depression is a prodromal manifestation of AD pathology.[60] These observations underscore the importance of investigating disease-specific vs. shared mechanisms underlying AHN alterations in neurodegenerative and psychiatric conditions. In this regard, our data show that human AHN and the DG neurogenic niche are differentially affected across distinct neuropsychiatric conditions and are further shaped by demographic and lifestyle-related factors (Figure 7). Although patients with neurodegenerative diseases[9] show generalized impairments in newborn DGC differentiation, those with neuropsychiatric diseases are more prominently affected in the initial AHN stages. Patients with MD and SCH showed a reduced density of NSCs, whereas those with all three conditions (MD, SCH, and BD) presented impaired NSC and neuroblast proliferation. The divergent patterns of AHN disruption across the diagnostic groups suggest that each condition engages unique cellular and molecular mechanisms. In MD, the preserved density and maturation ratios of immature DGCs point to a selective vulnerability of the early stages of AHN. In contrast, in SCH and BD, the increased densities of immature DGCs may reflect compensatory responses to reduced cell proliferation. Specifically, in SCH, the elevated early differentiation/proliferation ratio among immature DGCs could indicate enhanced early survival and/or prolongation of initial differentiation phases. In BD, the stability of both the early differentiation/proliferation and late/early differentiation ratios of DCX$^+$ DGCs

(C–N) Data stratified by biological sex (C)–(G) and alcohol consumption (H)–(N). (C) Density of DCX$^+$ calbindin (CB)$^+$ cells. (D) and (E) Percentage of DCX$^+$ polysialylated-neural cell adhesion molecule (PSA-NCAM)$^+$ (D) and DCX$^+$ CB$^+$ (E) out of total DCX$^+$ cells. (F) Orientation of neurites in DCX$^+$ cells. (G) Location of S100β$'$ astrocytes. (H)–(K) Location of HuC-HuD$^+$ (H) and (J) and PSA-NCAM$^+$ (I) and (K) cells. (L)–(N) Normalized length (L) and number of branches (M) and junctions (N) of *Ulex Europaeus* Agglutinin-I (UEA1)$^+$ capillaries in the granule cell layer (GCL).
F, female; M, male. n = 15 patients with MD. Graphs represent mean values ± SEM.
*$0.05 > p \geq 0.01$; **$0.01 > p \geq 0.001$; ***$p < 0.001$.
Detailed results of statistical comparisons are shown in Data S1.

Please cite this article in press as: Márquez-Valadez et al., Human adult hippocampal neurogenesis is shaped by neuropsychiatric disorders, demographics, and lifestyle-related factors, Cell Stem Cell (2025), https://doi.org/10.1016/j.stem.2025.08.010

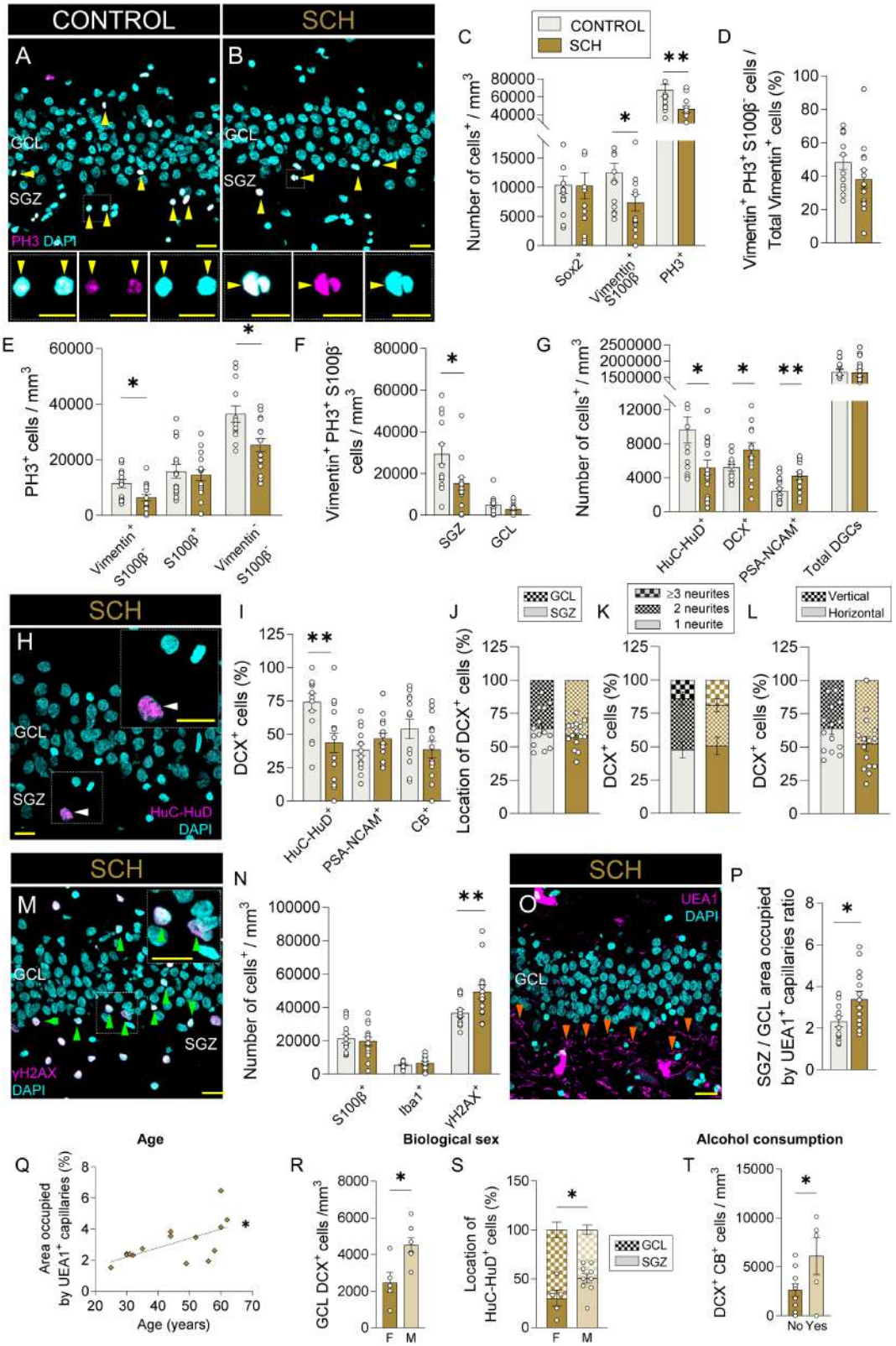

(legend on next page)

Please cite this article in press as: Márquez-Valadez et al., Human adult hippocampal neurogenesis is shaped by neuropsychiatric disorders, demographics, and lifestyle-related factors, Cell Stem Cell (2025), https://doi.org/10.1016/j.stem.2025.08.010

might instead reflect a generalized enhancement of immature DGC survival or a progressive impairment of neuronal maturation. Although functional studies are necessary to elucidate the role of immature DGCs in human hippocampal function, the distinctive neurophysiological properties and connectivity of these cells demonstrated in murine models[61,62] support the notion that the observed increase in cell densities and putative maturation arrest contributes to hippocampal-dependent cognitive and emotional impairments in these patients.

This potential functional significance highlights the importance of the DG neurogenic niche, a highly specialized microenvironment that tightly regulates the proliferation, differentiation, and synaptic integration of newborn DGCs, thereby sustaining hippocampal plasticity and function.[10] Similar to the mouse hippocampus,[10] the human SGZ is enriched with complex microcapillaries, dynamically shaped by blood flow[63] and brain metabolic demands.[64,65] These vessels establish a tri-dimensional plexus characterized by tight anatomical and functional interactions with neurons and glia.[66] Given the high metabolic demands of neurogenic niches, it is likely that active angiogenesis and vascular reabsorption[66] contribute to the great structural complexity of SGZ capillaries and their rapid functional adaptation. Human SGZ microcapillaries, like those in mice, differ from adjacent GCL vessels. This observation is consistent with mathematical models showing topological equivalence between mouse and human brain capillary networks.[67] The rapid adjustment of brain microvasculature in response to fluctuations in blood flow and neuronal metabolic demand is crucial in neurodegenerative diseases. In these conditions, vascular degeneration initiates early, with small vessel wall remodeling driven by mechanical stress and inflammation,[66,68,69] thereby disrupting endothelial-glial interactions.[66] Aging and neurodegenerative disorders are associated with vascular impairments,[24] including capillary occlusions, rarefaction,[70,71] reduced efficiency to regulate flow,[72,73] and compensatory vascular changes in the DG.[9] Notably, vascular alterations often precede clinical symptoms,[25] causing nutrient deficits that exacerbate disease progression and cognitive decline.[71,74] Although increased vascularization may facilitate nutrient and oxygen supply, it can also amplify pro-inflammatory signals.[9] Thus, the vascular alterations observed in psychiatric disorders are likely to compromise blood-brain barrier integrity and disrupt cellular interactions within the neurogenic niche, ultimately driving AHN impairments.

Considering the pivotal role of the neurogenic niche microenvironment, AHN is influenced by a complex interplay of intrinsic and extrinsic factors, including stress, sex hormones, and lifestyle-related factors. Epidemiological evidence consistently shows significant sex differences in the incidence and prevalence of mental disorders. Women are at higher risk of mood and anxiety disorders such as MD,[75,76] whereas SCH and substance use disorders are more common in men.[77] Although BD shows comparable lifetime prevalence across sexes, women experience a higher burden of depressive and hypomanic episodes, alongside increased rates of comorbidities.[78,79] These sex-specific patterns may reflect complex interactions among genetic, hormonal, psychosocial, and environmental influences that shape vulnerability and symptomatology throughout life.[75] Consistent with these findings, we observed that female subjects with neuropsychiatric conditions were more prone to showing further impairments in newborn neuron maturation and differentiation. In addition to female sex, advanced age, longer disease duration, early onset of disease, consumption of alcohol and/or drugs of abuse, presence of psychotic episodes, or death by suicide further aggravated alterations not only of AHN but also of the DG niche. To the best of our knowledge, this is the first study to address the differential impact of lifestyle-related factors, specifically alcohol consumption, on AHN and the neurogenic niche in neurologically healthy control subjects and patients with psychiatric disorders. Overall, alcohol intake influenced the differentiation of immature DGCs and the composition and spatial organization of the DG neurogenic niche. Notably, no dose-dependent effects of alcohol consumption were observed in healthy controls. Conversely, high consumption of alcohol exacerbated AHN impairments in patients with psychiatric conditions, particularly those diagnosed with MD.

Future research should address whether the described alterations in AHN and the DG niche are a causative factor of this disease or a consequence of other pathological mechanisms

Figure 5. AHN and DG neurogenic niche in patients with SCH

(A and B) Phospho-histone 3 $(PH3)^+$ cells in control subjects (A) and patients with SCH (B).
(C) Density of SRY (sex-determining region Y)-box 2 $(Sox2)^+$, $vimentin^+$ S100 calcium-binding protein B $(S100\beta)'$, and $PH3^+$ cells.
(D) Percentage of $vimentin^+$ cells that express PH3 but lack S100β expression out of the total number of $vimentin^+$ cells.
(E) Density of distinct subpopulations of $PH3^+$ cells.
(F) Density of $vimentin^+$ $PH3^+$ $S100\beta'$ in the granule cell layer (GCL) and the subgranular zone (SGZ).
(G) Density of $HuC\text{-}HuD^+$, doublecortin $(DCX)^+$, polysialylated-neural cell adhesion molecule $(PSA\text{-}NCAM)^+$, and total dentate granule cells (DGCs).
(H) $HuC\text{-}HuD^+$ proliferative neuroblasts.
(I) Percentage of DCX^+ immature DGCs that express Huc-HuD, PSA-NCAM, and calbindin (CB).
(J–L) Cell location (J) and number (K) and orientation (L) of neurites of DCX^+ cells.
(M) Phosphorylated H2AX (γH2AX) staining.
(N) Density of $S100\beta^+$, $Iba1^+$, and $\gamma H2AX^+$ cells.
(O) Vascularization of the DG.
(P) Normalized ratio of the SGZ/GCL area occupied by *Ulex Europaeus* Agglutinin-I $(UEA1)^+$ capillaries.
(Q–T) Statistically significant data obtained from patients with SCH. Data stratified by age (Q), biological sex (R) and (S), and alcohol consumption (T). (Q) Correlation between the age of the subject and the area occupied by $UEA1^+$ capillaries. (R) Density of DCX^+ cells in the GCL. (S) Location of $HuC\text{-}HuD^+$ cells. (T) Density of DCX^+ CB^+ cells.
F, female; M, male. $n = 14$ neurologically healthy control subjects and 15 patients with SCH. Graphs represent mean values ± SEM. Yellow scale bar: 20 μm. Yellow triangles: $PH3^+$ cells. White triangles: $HuC\text{-}HuD^+$ neuroblasts. Green triangles: $\gamma H2AX^+$ cells. Orange triangles: capillaries.
$^*0.05 > p \geq 0.01$; $^{**}0.01 > p \geq 0.001$.
Detailed results of statistical comparisons are shown in Data S1.

Please cite this article in press as: Márquez-Valadez et al., Human adult hippocampal neurogenesis is shaped by neuropsychiatric disorders, demographics, and lifestyle-related factors, Cell Stem Cell (2025), https://doi.org/10.1016/j.stem.2025.08.010

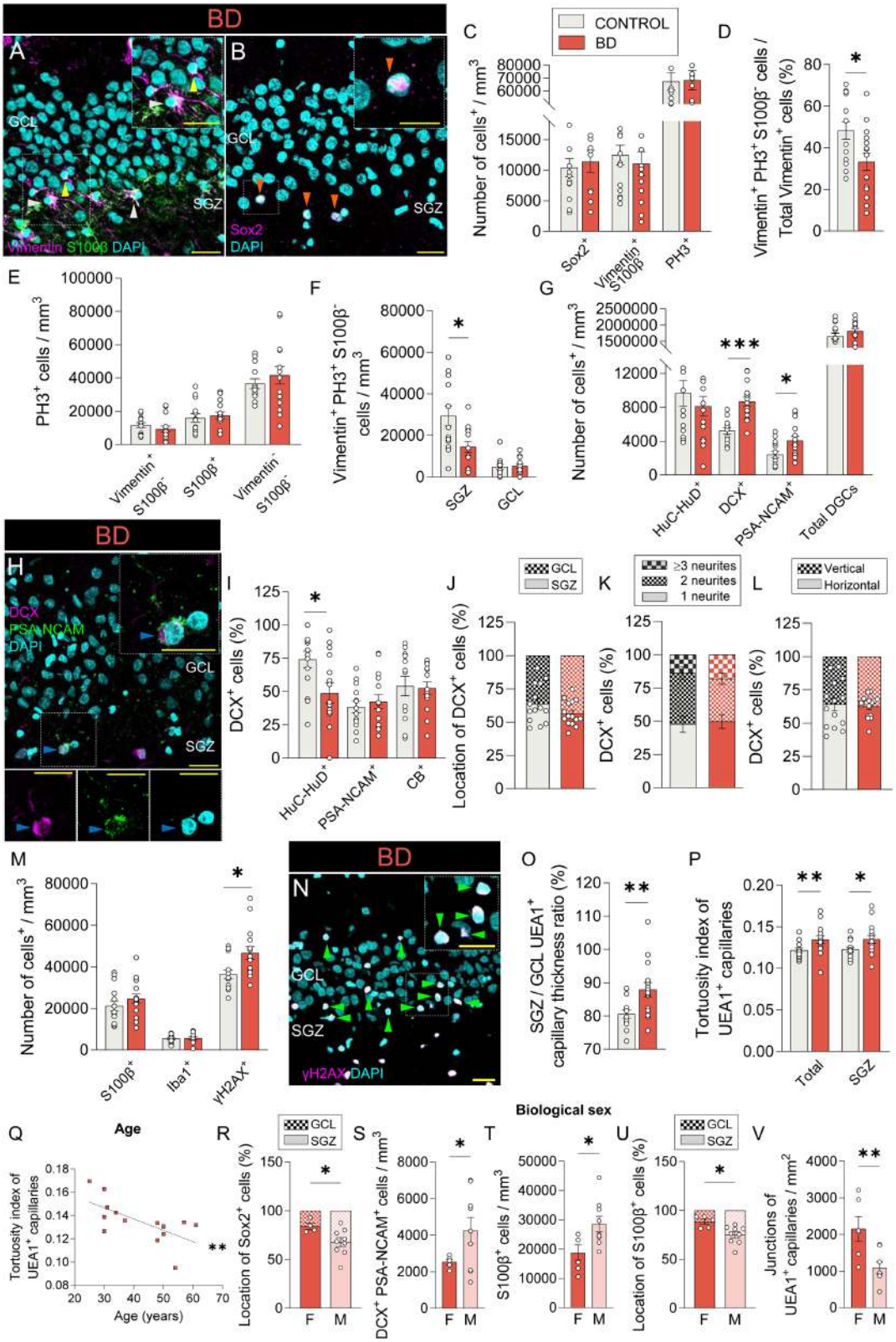

(legend on next page)

driving psychiatric disorders. In this context, it will be critical to determine the extent to which differences in AHN alterations between neurodegenerative and psychiatric disorders—where immature neurons and early proliferative stages, respectively, appear to be predominantly affected—reflect distinct underlying mechanisms. Furthermore, whether disruptions in the neurogenic niche itself constitute an underlying cause of impaired AHN remains to be elucidated. These questions are especially pertinent in light of the growing recognition of human-specific aspects of AHN and the limited translational validity of current preclinical models, especially in the context of psychiatric conditions. This study underscores not only the biological and clinical relevance of human AHN and the DG neurogenic niche but also the exceptional challenge of obtaining high-quality human brain samples—an indispensable resource for bridging the gap between experimental models and human disease. Notably, the observation that AHN and the DG neurogenic niche are influenced not only by disease state but also by demographic variables (such as biological sex and age) and modifiable lifestyle factors suggests that these parameters should be carefully considered in the design of future therapeutic strategies targeting neuroplasticity in the human brain.

Limitations of the study

This is, to the best of our knowledge, the first study to systematically examine the effects of psychiatric disorders, demographic variables, and selected lifestyle-related factors on AHN dynamics and the structural integrity of the DG neurogenic niche. However, as with all studies based on post-mortem human tissue, certain experimental constraints must be acknowledged. First, the availability of high-quality, well-preserved human brain samples is inherently limited. Moreover, as previously discussed in detail,[80,81] certain antibodies (e.g., the anti-nestin antibody used in Terreros-Roncal et al.[9]) may not be compatible with specific tissue processing protocols (e.g., with the use of Triton X-100 as a permeabilizing agent). As a result, the use of different marker combinations to delineate specific cell populations can contribute to apparent discrepancies in reported cell counts and densities across studies.[80,81] These technical considerations, along with variability in the stereological methods applied, may hinder direct cross-study comparisons.[81]

In addition, research based on post-mortem material—including the present work—is inherently limited in its capacity to explore mechanistic relationships. Nonetheless, the inclusion of comprehensive antemortem data and clinical metadata represents a critical step toward contextualizing and interpreting immunohistochemical observations, as emphasized previously.[80,81] Finally, although this study integrates multiple lifestyle-related variables, lifestyle is a complex, multidimensional construct that cannot be fully captured through a limited number of discrete categories. The relatively small sample size within some of the subgroups examined, as well as the practical limitations in fully balancing demographic and diagnostic variables across all groups, may have constrained our ability to detect more subtle associations. Future studies with larger, stratified cohorts and more detailed characterization of lifestyle components—such as dietary habits, physical activity, stress exposure, and sleep patterns—will be essential to refine our understanding of how modifiable behaviors influence AHN and the human neurogenic niche.

RESOURCE AVAILABILITY

Lead contact

Further information and requests for resources and reagents should be directed to, and will be fulfilled by, the lead contact, María Llorens-Martín (m.llorens@csic.es).

Materials availability

No original materials have been generated in this study. Requests for human brain samples should be addressed to the Stanley Medical Research Institute (https://stanleyresearch.org).

Data and code availability

- All the raw data generated are included in Table S1.
- This paper does not report original code.
- Any additional information required to reanalyze the data reported in this paper is available from the lead contact upon reasonable request.

Figure 6. AHN and DG neurogenic niche in patients with BD

(A) Vimentin$^+$ S100 calcium-binding protein B (S100β)$^-$ NSCs and vimentin$^+$ S100β$^+$ astrocytes.
(B) SRY (sex-determining region Y)-box 2 (Sox2)$^+$ cells.
(C) Density of Sox2$^+$, vimentin$^+$ S100β$^-$, and phospho-histone 3 (PH3)$^+$ cells.
(D) Percentage of vimentin$^+$ cells that express PH3 but lack S100β expression out of the total number of vimentin$^+$ cells.
(E) Density of distinct subpopulations of PH3$^+$ cells.
(F) Density of vimentin$^+$ PH3$^+$ S100β$^-$ in the granule cell layer (GCL) and the subgranular zone (SGZ).
(G) Density of HuC-HuD$^+$, doublecortin (DCX)$^+$, polysialylated-neural cell adhesion molecule (PSA-NCAM)$^+$, and total dentate granule cells (DGCs).
(H) DCX$^+$ PSA-NCAM$^+$ immature DGC.
(I) Percentage of DCX$^+$ immature DGCs that express Huc-HuD, PSA-NCAM, and calbindin (CB).
(J–L) Cell location (J) and number (K) and orientation (L) of neurites of DCX$^+$ cells.
(M) Density of S100β$^+$, Iba1$^+$, and phosphorylated H2AX (γH2AX)$^+$ cells.
(N) γH2AX staining.
(O) SGZ/GCL capillary thickness ratio of *Ulex Europaeus* Agglutinin-I (UEA1)$^+$ capillaries.
(P) Tortuosity index of total and SGZ UEA1$^+$ capillaries.
(Q–V) Statistically significant data obtained from patients with SCH. Data stratified by age (Q) and biological sex (R)–(V). (Q) Correlation between the age of the subject and the tortuosity of UEA1$^+$ capillaries. (R) Location of Sox2$^+$ cells. (S) Density of DCX$^+$ PSA-NCAM$^+$ cells. (T) and (U) Density (T) and location (U) of S100β$^+$ cells. (V) Number of junctions of UEA1$^+$ capillaries.
F, female; M, male. $n = 14$ neurologically healthy control subjects and 15 patients with BD. Graphs represent mean values ± SEM. Yellow scale bar: 20 μm. Yellow triangle: NSC. White triangles: astrocytes. Orange triangle: Sox2$^+$ cell. Blue triangle: neuroblast. Green triangles: γH2AX$^+$ cells.
*$0.05 > p \geq 0.01$; **$0.01 > p \geq 0.001$; ***$p < 0.001$.
Detailed results of statistical comparisons are shown in Data S1.

Please cite this article in press as: Márquez-Valadez et al., Human adult hippocampal neurogenesis is shaped by neuropsychiatric disorders, demographics, and lifestyle-related factors, Cell Stem Cell (2025), https://doi.org/10.1016/j.stem.2025.08.010

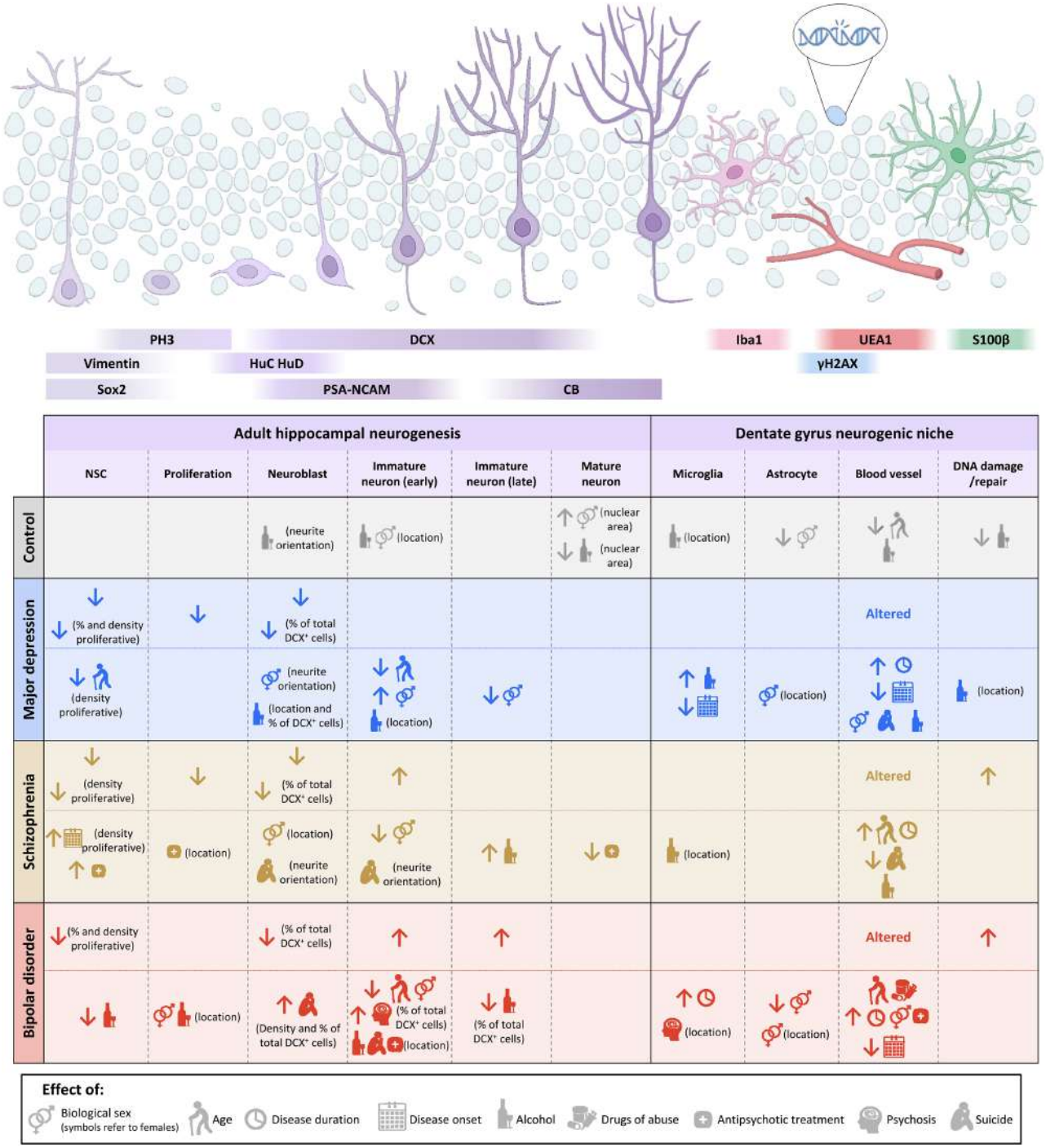

Figure 7. Schematic summary illustrating the neurogenic stages and components of the DG neurogenic niche affected by each neuropsychiatric condition and key demographic/lifestyle variables

PH3, phospho-histone 3; DCX, doublecortin; Sox2, SRY (sex-determining region Y)-box 2; PSA-NCAM, polysialylated-neural cell adhesion molecule; UEA1, *Ulex Europaeus* Agglutinin-I; γH2AX, phosphorylated H2AX; S100β, S100 calcium-binding protein B; NSC, neural stem cell.

ACKNOWLEDGMENTS

The authors would like to thank the patients and their families for generously donating brain samples. Moreover, they wish to thank the SMRI brain bank for providing samples and J. Molina-Hernández, M. Flor-García, J. Terreros-Roncal, E. Moreno-Jiménez, C. Rodríguez-Moreno, and the Confocal Microscopy Facility at the CBMSO for technical assistance. They also thank M.J. Webster for help with human sample requests and critical revision of the manuscript.

This study was supported by The European Research Council (ERC) (ERC-CoG-2020-101001916) (M.L.-M.), the Spanish Ministry of Economy and

Competitiveness (PID2020-113007RB-I00 and PID2023-146572OB-I00) (M.L.-M.), the BrightFocus Foundation (A2024021S) (M.L.-M.), and the Center for Networked Biomedical Research on Neurodegenerative Diseases (CIBERNED, Spain) (M.L.-M.). The salary of B.M.-V. was supported by postdoctoral fellowships awarded by the Consejo Nacional de Ciencia y Tecnología (CONACYT) of the Mexican Government (385084) and the Secretaria de Educación, Ciencia Tecnología e Innovación (SECTEI) of the Regional Government of Ciudad de México (CDMX) (CM-SECTEI/159/2021). The salary of M.G.-C. was supported by a Formación de Personal Investigador (FPI) contract, associated with the PID2020-113007RB-I00 grant (M.L.-M.), awarded by the Spanish Ministry of Economy and Competitiveness (PRE2021-097690).

AUTHOR CONTRIBUTIONS

B.M.-V., M.G.-C., and M.L.-M. conceived and designed the study. B.M.-V. and M.G.-C. performed the experiments. The Stanley Medical Research Institute provided the brain samples. B.M.-V., M.G.-C. and M.L.-M. analyzed the data, designed the figures, and wrote the manuscript. B.M.-V. and M.L.-M. obtained the funding. All the authors discussed the data and revised the final version of the manuscript.

DECLARATION OF INTERESTS

The authors declare no competing interests.

STAR★METHODS

Detailed methods are provided in the online version of this paper and include the following:

- KEY RESOURCES TABLE
- EXPERIMENTAL MODEL AND STUDY PARTICIPANT DETAILS
- METHOD DETAILS
  - Tissue collection and storage
  - Tissue fixation
  - Immunohistochemistry
  - Confocal microscopy
- QUANTIFICATION AND STATISTICAL ANALYSIS
  - Stereological cell counts
  - Calculation of cell ratios
  - Morphometric determinations
  - Analysis of the dentate gyrus (DG) vasculature
  - Statistical analyses

SUPPLEMENTAL INFORMATION

Supplemental information can be found online at https://doi.org/10.1016/j.stem.2025.08.010.

Received: March 13, 2025
Revised: June 27, 2025
Accepted: August 11, 2025

REFERENCES

1. Altman, J. (1963). Autoradiographic investigation of cell proliferation in the brains of rats and cats. Anat. Rec. *145*, 573–591. https://doi.org/10.1002/ar.1091450409.
2. Eriksson, P.S., Perfilieva, E., Björk-Eriksson, T., Alborn, A.M., Nordborg, C., Peterson, D.A., and Gage, F.H. (1998). Neurogenesis in the adult human hippocampus. Nat. Med. *4*, 1313–1317. https://doi.org/10.1038/3305.
3. Hill, A.S., Sahay, A., and Hen, R. (2015). Increasing Adult Hippocampal Neurogenesis is Sufficient to Reduce Anxiety and Depression-Like Behaviors. Neuropsychopharmacology *40*, 2368–2378. https://doi.org/10.1038/npp.2015.85.
4. Sahay, A., Scobie, K.N., Hill, A.S., O'Carroll, C.M., Kheirbek, M.A., Burghardt, N.S., Fenton, A.A., Dranovsky, A., and Hen, R. (2011). Increasing adult hippocampal neurogenesis is sufficient to improve pattern separation. Nature *472*, 466–470. https://doi.org/10.1038/nature09817.
5. Akers, K.G., Martinez-Canabal, A., Restivo, L., Yiu, A.P., De Cristofaro, A., Hsiang, H.L.L., Wheeler, A.L., Guskjolen, A., Niibori, Y., Shoji, H., et al. (2014). Hippocampal neurogenesis regulates forgetting during adulthood and infancy. Science *344*, 598–602. https://doi.org/10.1126/science.1248903.
6. Zhou, Y., Su, Y., Li, S., Kennedy, B.C., Zhang, D.Y., Bond, A.M., Sun, Y., Jacob, F., Lu, L., Hu, P., et al. (2022). Molecular landscapes of human hippocampal immature neurons across lifespan. Nature *607*, 527–533. https://doi.org/10.1038/s41586-022-04912-w.
7. Dumitru, I., Paterlini, M., Zamboni, M., Ziegenhain, C., Giatrellis, S., Saghaleyni, R., Björklund, Å., Alkass, K., Tata, M., Druid, H., et al. (2025). Identification of proliferating neural progenitors in the adult human hippocampus. Science *389*, 58–63. https://doi.org/10.1126/science.adu9575.
8. Moreno-Jiménez, E.P., Flor-García, M., Terreros-Roncal, J., Rábano, A., Cafini, F., Pallas-Bazarra, N., Ávila, J., and Llorens-Martín, M. (2019). Adult hippocampal neurogenesis is abundant in neurologically healthy subjects and drops sharply in patients with Alzheimer's disease. Nat. Med. *25*, 554–560. https://doi.org/10.1038/s41591-019-0375-9.
9. Terreros-Roncal, J., Moreno-Jiménez, E.P., Flor-García, M., Rodríguez-Moreno, C.B., Trinchero, M.F., Cafini, F., Rábano, A., and Llorens-Martín, M. (2021). Impact of neurodegenerative diseases on human adult hippocampal neurogenesis. Science *374*, 1106–1113. https://doi.org/10.1126/science.abl5163.
10. Vicidomini, C., Guo, N., and Sahay, A. (2020). Communication, Cross Talk, and Signal Integration in the Adult Hippocampal Neurogenic Niche. Neuron *105*, 220–235. https://doi.org/10.1016/j.neuron.2019.11.029.
11. Sierra, A., Encinas, J.M., Deudero, J.J.P., Chancey, J.H., Enikolopov, G., Overstreet-Wadiche, L.S., Tsirka, S.E., and Maletic-Savatic, M. (2010). Microglia shape adult hippocampal neurogenesis through apoptosis-coupled phagocytosis. Cell Stem Cell *7*, 483–495. https://doi.org/10.1016/j.stem.2010.08.014.
12. Sultan, S., Li, L., Moss, J., Petrelli, F., Cassé, F., Gebara, E., Lopatar, J., Pfrieger, F.W., Bezzi, P., Bischofberger, J., and Toni, N. (2015). Synaptic Integration of Adult-Born Hippocampal Neurons Is Locally Controlled by Astrocytes. Neuron *88*, 957–972. https://doi.org/10.1016/j.neuron.2015.10.037.
13. Frodl, T., Meisenzahl, E.M., Zetzsche, T., Born, C., Groll, C., Jäger, M., Leinsinger, G., Bottlender, R., Hahn, K., and Möller, H.J. (2002). Hippocampal changes in patients with a first episode of major depression. Am. J. Psychiatry *159*, 1112–1118. https://doi.org/10.1176/appi.ajp.159.7.1112.
14. van Erp, T.G.M., Thompson, P.M., Kieseppä, T., Bearden, C.E., Marino, A.C., Hoftman, G.D., Haukka, J., Partonen, T., Huttunen, M., Kaprio, J., et al. (2012). Hippocampal morphology in lithium and non-lithium-treated bipolar I disorder patients, non-bipolar co-twins, and control twins. Hum. Brain Mapp. *33*, 501–510. https://doi.org/10.1002/hbm.21239.
15. Hajek, T., Kopecek, M., Höschl, C., and Alda, M. (2012). Smaller hippocampal volumes in patients with bipolar disorder are masked by exposure to lithium: a meta-analysis. J. Psychiatry Neurosci. *37*, 333–343. https://doi.org/10.1503/jpn.110143.
16. Duan, X., Chang, J.H., Ge, S., Faulkner, R.L., Kim, J.Y., Kitabatake, Y., Liu, X.B., Yang, C.H., Jordan, J.D., Ma, D.K., et al. (2007). Disrupted-In-Schizophrenia 1 regulates integration of newly generated neurons in the adult brain. Cell *130*, 1146–1158. https://doi.org/10.1016/j.cell.2007.07.010.
17. Lazarov, O., Disouky, A., Sanborn, M., Mostafa, M., Sabitha, K., Schantz, A., Kim, N., Pawlowski, S., Honer, W., Bennett, D., et al. (2024). A roadmap to human hippocampal neurogenesis in adulthood, aging and AD. Preprint at Res Sq. https://doi.org/10.21203/rs.3.rs-4469965/v1.

18. Encinas, J.M., and Enikolopov, G. (2008). Identifying and quantitating neural stem and progenitor cells in the adult brain. Methods Cell Biol. *85*, 243–272. https://doi.org/10.1016/S0091-679X(08)85011-X.

19. Harris, L., Rigo, P., Stiehl, T., Gaber, Z.B., Austin, S.H.L., Masdeu, M.D.M., Edwards, A., Urbán, N., Marciniak-Czochra, A., and Guillemot, F. (2021). Coordinated changes in cellular behavior ensure the lifelong maintenance of the hippocampal stem cell population. Cell Stem Cell *28*, 863–876.e6. https://doi.org/10.1016/j.stem.2021.01.003.

20. Bottes, S., Jaeger, B.N., Pilz, G.A., Jörg, D.J., Cole, J.D., Kruse, M., Harris, L., Korobeynyk, V.I., Mallona, I., Helmchen, F., et al. (2021). Long-term self-renewing stem cells in the adult mouse hippocampus identified by intravital imaging. Nat. Neurosci. *24*, 225–233. https://doi.org/10.1038/s41593-020-00759-4.

21. Del Castillo, P., Llorente, A.R., and Stockert, J.C. (1989). Influence of fixation, exciting light and section thickness on the primary fluorescence of samples for microfluorometric analysis. Basic Appl. Histochem. *33*, 251–257.

22. Kempermann, G., Jessberger, S., Steiner, B., and Kronenberg, G. (2004). Milestones of neuronal development in the adult hippocampus. Trends Neurosci. *27*, 447–452. https://doi.org/10.1016/j.tins.2004.05.013.

23. Stolp, H.B., and Molnár, Z. (2015). Neurogenic niches in the brain: help and hindrance of the barrier systems. Front. Neurosci. *9*, 20. https://doi.org/10.3389/fnins.2015.00020.

24. Boldrini, M., Fulmore, C.A., Tartt, A.N., Simeon, L.R., Pavlova, I., Poposka, V., Rosoklija, G.B., Stankov, A., Arango, V., Dwork, A.J., et al. (2018). Human Hippocampal Neurogenesis Persists throughout Aging. Cell Stem Cell *22*, 589–599.e5. https://doi.org/10.1016/j.stem.2018.03.015.

25. Sun, Z., Li, C., Wisniewski, T.W., Haacke, E.M., and Ge, Y. (2024). In Vivo Detection of Age-Related Tortuous Cerebral Small Vessels using Ferumoxytol-enhanced 7T MRI. Aging Dis. *15*, 1913–1926. https://doi.org/10.14336/AD.2023.1110-1.

26. Spalding, K.L., Bergmann, O., Alkass, K., Bernard, S., Salehpour, M., Huttner, H.B., Boström, E., Westerlund, I., Vial, C., Buchholz, B.A., et al. (2013). Dynamics of hippocampal neurogenesis in adult humans. Cell *153*, 1219–1227. https://doi.org/10.1016/j.cell.2013.05.002.

27. Tanapat, P., Hastings, N.B., Reeves, A.J., and Gould, E. (1999). Estrogen stimulates a transient increase in the number of new neurons in the dentate gyrus of the adult female rat. J. Neurosci. *19*, 5792–5801. https://doi.org/10.1523/JNEUROSCI.19-14-05792.1999.

28. Wang, Q., Van Heerikhuize, J., Aronica, E., Kawata, M., Seress, L., Joels, M., Swaab, D.F., and Lucassen, P.J. (2013). Glucocorticoid receptor protein expression in human hippocampus; stability with age. Neurobiol. Aging *34*, 1662–1673. https://doi.org/10.1016/j.neurobiolaging.2012.11.019.

29. Guebel, D.V. (2023). Human hippocampal astrocytes: Computational dissection of their transcriptome, sexual differences and exosomes across ageing and mild-cognitive impairment. Eur. J. Neurosci. *58*, 2677–2707. https://doi.org/10.1111/ejn.16081.

30. Mah, L.J., El-Osta, A., and Karagiannis, T.C. (2010). gammaH2AX: a sensitive molecular marker of DNA damage and repair. Leukemia *24*, 679–686. https://doi.org/10.1038/leu.2010.6.

31. Le Maître, T.W., Dhanabalan, G., Bogdanovic, N., Alkass, K., and Druid, H. (2018). Effects of Alcohol Abuse on Proliferating Cells, Stem/Progenitor Cells, and Immature Neurons in the Adult Human Hippocampus. Neuropsychopharmacology *43*, 690–699. https://doi.org/10.1038/npp.2017.251.

32. Dhanabalan, G., Le Maître, T.W., Bogdanovic, N., Alkass, K., and Druid, H. (2018). Hippocampal granule cell loss in human chronic alcohol abusers. Neurobiol. Dis. *120*, 63–75. https://doi.org/10.1016/j.nbd.2018.08.011.

33. Campbell, S., Marriott, M., Nahmias, C., and MacQueen, G.M. (2004). Lower hippocampal volume in patients suffering from depression: a meta-analysis. Am. J. Psychiatry *161*, 598–607. https://doi.org/10.1176/appi.ajp.161.4.598.

34. Santarelli, L., Saxe, M., Gross, C., Surget, A., Battaglia, F., Dulawa, S., Weisstaub, N., Lee, J., Duman, R., Arancio, O., et al. (2003). Requirement of hippocampal neurogenesis for the behavioral effects of antidepressants. Science *301*, 805–809. https://doi.org/10.1126/science.1083328.

35. Duman, R.S., Malberg, J., Nakagawa, S., and D'Sa, C. (2000). Neuronal plasticity and survival in mood disorders. Biol. Psychiatry *48*, 732–739. https://doi.org/10.1016/s0006-3223(00)00935-5.

36. Reif, A., Fritzen, S., Finger, M., Strobel, A., Lauer, M., Schmitt, A., and Lesch, K.P. (2006). Neural stem cell proliferation is decreased in schizophrenia, but not in depression. Mol. Psychiatry *11*, 514–522. https://doi.org/10.1038/sj.mp.4001791.

37. Boldrini, M., Hen, R., Underwood, M.D., Rosoklija, G.B., Dwork, A.J., Mann, J.J., and Arango, V. (2012). Hippocampal angiogenesis and progenitor cell proliferation are increased with antidepressant use in major depression. Biol. Psychiatry *72*, 562–571. https://doi.org/10.1016/j.biopsych.2012.04.024.

38. Lucassen, P.J., Stumpel, M.W., Wang, Q., and Aronica, E. (2010). Decreased numbers of progenitor cells but no response to antidepressant drugs in the hippocampus of elderly depressed patients. Neuropharmacology *58*, 940–949. https://doi.org/10.1016/j.neuropharm.2010.01.012.

39. Boldrini, M., Underwood, M.D., Hen, R., Rosoklija, G.B., Dwork, A.J., John Mann, J., and Arango, V. (2009). Antidepressants increase neural progenitor cells in the human hippocampus. Neuropsychopharmacology *34*, 2376–2389. https://doi.org/10.1038/npp.2009.75.

40. Epp, J.R., Beasley, C.L., and Galea, L.A. (2013). Increased hippocampal neurogenesis and p21 expression in depression: dependent on antidepressants, sex, age, and antipsychotic exposure. Neuropsychopharmacology *38*, 2297–2306. https://doi.org/10.1038/npp.2013.132.

41. Boldrini, M., Santiago, A.N., Hen, R., Dwork, A.J., Rosoklija, G.B., Tamir, H., Arango, V., and John Mann, J. (2013). Hippocampal granule neuron number and dentate gyrus volume in antidepressant-treated and untreated major depression. Neuropsychopharmacology *38*, 1068–1077. https://doi.org/10.1038/npp.2013.5.

42. Li, D.J., Tsai, S.J., Chen, T.J., Kao, Y.C., Liang, C.S., and Chen, M.H. (2025). The association of sex and age of treatment-resistant tendency to antidepressants: A cohort study of 325,615 patients with major depressive disorder. J. Affect. Disord. *382*, 248–255. https://doi.org/10.1016/j.jad.2025.04.071.

43. Mahajan, G.J., Vallender, E.J., Garrett, M.R., Challagundla, L., Overholser, J.C., Jurjus, G., Dieter, L., Syed, M., Romero, D.G., Benghuzzi, H., and Stockmeier, C.A. (2018). Altered neuro-inflammatory gene expression in hippocampus in major depressive disorder. Prog. Neuropsychopharmacol. Biol. Psychiatry *82*, 177–186. https://doi.org/10.1016/j.pnpbp.2017.11.017.

44. Patton, N., Aslam, T.M., MacGillivray, T., Deary, I.J., Dhillon, B., Eikelboom, R.H., Yogesan, K., and Constable, I.J. (2006). Retinal image analysis: concepts, applications and potential. Prog. Retin. Eye Res. *25*, 99–127. https://doi.org/10.1016/j.preteyeres.2005.07.001.

45. Burrage, E., Marshall, K.L., Santanam, N., and Chantler, P.D. (2018). Cerebrovascular dysfunction with stress and depression. Brain Circ. *4*, 43–53. https://doi.org/10.4103/bc.bc_6_18.

46. Heckers, S., Rauch, S.L., Goff, D., Savage, C.R., Schacter, D.L., Fischman, A.J., and Alpert, N.M. (1998). Impaired recruitment of the hippocampus during conscious recollection in schizophrenia. Nat. Neurosci. *1*, 318–323. https://doi.org/10.1038/1137.

47. Nelson, M.D., Saykin, A.J., Flashman, L.A., and Riordan, H.J. (1998). Hippocampal volume reduction in schizophrenia as assessed by magnetic resonance imaging: a meta-analytic study. Arch. Gen. Psychiatry *55*, 433–440. https://doi.org/10.1001/archpsyc.55.5.433.

48. Wang, K., Li, X., Wang, X., Hommel, B., Xia, X., Qiu, J., Fu, Y., and Zhou, Z. (2023). In vivo analyses reveal hippocampal subfield volume reductions in adolescents with schizophrenia, but not with major depressive disorder. J. Psychiatr. Res. *165*, 56–63. https://doi.org/10.1016/j.jpsychires.2023.07.012.

49. Silbersweig, D.A., Stern, E., Frith, C., Cahill, C., Holmes, A., Grootoonk, S., Seaward, J., McKenna, P., Chua, S.E., Schnorr, L., et al. (1995). A functional neuroanatomy of hallucinations in schizophrenia. Nature *378*, 176–179. https://doi.org/10.1038/378176a0.

50. Heckers, S., Heinsen, H., Geiger, B., and Beckmann, H. (1991). Hippocampal neuron number in schizophrenia. A stereological study. Arch. Gen. Psychiatry *48*, 1002–1008. https://doi.org/10.1001/archpsyc.1991.01810350042006.

51. Allen, K.M., Fung, S.J., and Weickert, C.S. (2016). Cell proliferation is reduced in the hippocampus in schizophrenia. Aust. N. Z. J. Psychiatry *50*, 473–480. https://doi.org/10.1177/0004867415589793.

52. Katsel, P., Roussos, P., Pletnikov, M., and Haroutunian, V. (2017). Microvascular anomaly conditions in psychiatric disease. Schizophrenia - angiogenesis connection. Neurosci. Biobehav. Rev. *77*, 327–339. https://doi.org/10.1016/j.neubiorev.2017.04.003.

53. Appaji, A., Nagendra, B., Chako, D.M., Padmanabha, A., Jacob, A., Hiremath, C.V., Varambally, S., Kesavan, M., Venkatasubramanian, G., Rao, S.V., et al. (2019). Retinal vascular tortuosity in schizophrenia and bipolar disorder. Schizophr. Res. *212*, 26–32. https://doi.org/10.1016/j.schres.2019.08.020.

54. Rubin, E., Sackeim, H.A., Prohovnik, I., Moeller, J.R., Schnur, D.B., and Mukherjee, S. (1995). Regional cerebral blood flow in mood disorders: IV. Comparison of mania and depression. Psychiatry Res. *61*, 1–10. https://doi.org/10.1016/0925-4927(95)02594-n.

55. Mathew, R.J., Wilson, W.H., Tant, S.R., Robinson, L., and Prakash, R. (1988). Abnormal resting regional cerebral blood flow patterns and their correlates in schizophrenia. Arch. Gen. Psychiatry *45*, 542–549. https://doi.org/10.1001/archpsyc.1988.01800300038004.

56. Walton, N.M., Zhou, Y., Kogan, J.H., Shin, R., Webster, M., Gross, A.K., Heusner, C.L., Chen, Q., Miyake, S., Tajinda, K., et al. (2012). Detection of an immature dentate gyrus feature in human schizophrenia/bipolar patients. Transl. Psychiatry *2*, e135. https://doi.org/10.1038/tp.2012.56.

57. Goldstein, B.I. (2017). Bipolar Disorder and the Vascular System: Mechanisms and New Prevention Opportunities. Can. J. Cardiol. *33*, 1565–1576. https://doi.org/10.1016/j.cjca.2017.10.006.

58. Toma, S., MacIntosh, B.J., Swardfager, W., and Goldstein, B.I. (2018). Cerebral blood flow in bipolar disorder: A systematic review. J. Affect. Disord. *241*, 505–513. https://doi.org/10.1016/j.jad.2018.08.040.

59. Du Preez, A., Lefèvre-Arbogast, S., González-Domínguez, R., Houghton, V., de Lucia, C., Lee, H., Low, D.Y., Helmer, C., Féart, C., Delcourt, C., et al. (2024). Association of dietary and nutritional factors with cognitive decline, dementia, and depressive symptomatology in older individuals according to a neurogenesis-centred biological susceptibility to brain ageing. Age Ageing *53*, ii47–ii59. https://doi.org/10.1093/ageing/afae042.

60. Berger, T., Lee, H., Young, A.H., Aarsland, D., and Thuret, S. (2020). Adult Hippocampal Neurogenesis in Major Depressive Disorder and Alzheimer's Disease. Trends Mol. Med. *26*, 803–818. https://doi.org/10.1016/j.molmed.2020.03.010.

61. Kee, N., Teixeira, C.M., Wang, A.H., and Frankland, P.W. (2007). Preferential incorporation of adult-generated granule cells into spatial memory networks in the dentate gyrus. Nat. Neurosci. *10*, 355–362. https://doi.org/10.1038/nn1847.

62. Luna, V.M., Anacker, C., Burghardt, N.S., Khandaker, H., Andreu, V., Millette, A., Leary, P., Ravenelle, R., Jimenez, J.C., Mastrodonato, A., et al. (2019). Adult-born hippocampal neurons bidirectionally modulate entorhinal inputs into the dentate gyrus. Science *364*, 578–583. https://doi.org/10.1126/science.aat8789.

63. Chen, Q., Jiang, L., Li, C., Hu, D., Bu, J.W., Cai, D., and Du, J.L. (2012). Haemodynamics-driven developmental pruning of brain vasculature in zebrafish. PLoS Biol. *10*, e1001374. https://doi.org/10.1371/journal.pbio.1001374.

64. Lacoste, B., Comin, C.H., Ben-Zvi, A., Kaeser, P.S., Xu, X., Costa, Lda F., and Gu, C. (2014). Sensory-related neural activity regulates the structure of vascular networks in the cerebral cortex. Neuron *83*, 1117–1130. https://doi.org/10.1016/j.neuron.2014.07.034.

65. Hartmann, D.A., Berthiaume, A.A., Grant, R.I., Harrill, S.A., Koski, T., Tieu, T., McDowell, K.P., Faino, A.V., Kelly, A.L., and Shih, A.Y. (2021). Brain capillary pericytes exert a substantial but slow influence on blood flow. Nat. Neurosci. *24*, 633–645. https://doi.org/10.1038/s41593-020-00793-2.

66. Marín-Padilla, M. (2012). The human brain intracerebral microvascular system: development and structure. Front. Neuroanat. *6*, 38. https://doi.org/10.3389/fnana.2012.00038.

67. Smith, A.F., Doyeux, V., Berg, M., Peyrounette, M., Haft-Javaherian, M., Larue, A.E., Slater, J.H., Lauwers, F., Blinder, P., Tsai, P., et al. (2019). Brain Capillary Networks Across Species: A few Simple Organizational Requirements Are Sufficient to Reproduce Both Structure and Function. Front. Physiol. *10*, 233. https://doi.org/10.3389/fphys.2019.00233.

68. Wang, J., Lu, J., Qi, P., Li, C., Yang, X., Chen, K., and Wang, D. (2022). Association between kinking of the cervical carotid or vertebral artery and ischemic stroke/TIA. Front. Neurol. *13*, 1008328. https://doi.org/10.3389/fneur.2022.1008328.

69. Togay-Işikay, C., Kim, J., Betterman, K., Andrews, C., Meads, D., Tesh, P., Tegeler, C., and Oztuna, D. (2005). Carotid artery tortuosity, kinking, coiling: stroke risk factor, marker, or curiosity? Acta Neurol. Belg. *105*, 68–72.

70. Østergaard, L., Engedal, T.S., Moreton, F., Hansen, M.B., Wardlaw, J.M., Dalkara, T., Markus, H.S., and Muir, K.W. (2016). Cerebral small vessel disease: Capillary pathways to stroke and cognitive decline. J. Cereb. Blood Flow Metab. *36*, 302–325. https://doi.org/10.1177/0271678X15606723.

71. Cruz Hernández, J.C., Bracko, O., Kersbergen, C.J., Muse, V., Haft-Javaherian, M., Berg, M., Park, L., Vinarcsik, L.K., Ivasyk, I., Rivera, D.A., et al. (2019). Neutrophil adhesion in brain capillaries reduces cortical blood flow and impairs memory function in Alzheimer's disease mouse models. Nat. Neurosci. *22*, 413–420. https://doi.org/10.1038/s41593-018-0329-4.

72. Farkas, E., and Luiten, P.G. (2001). Cerebral microvascular pathology in aging and Alzheimer's disease. Prog. Neurobiol. *64*, 575–611. https://doi.org/10.1016/s0301-0082(00)00068-x.

73. Iadecola, C. (2004). Neurovascular regulation in the normal brain and in Alzheimer's disease. Nat. Rev. Neurosci. *5*, 347–360. https://doi.org/10.1038/nrn1387.

74. Zlokovic, B.V. (2011). Neurovascular pathways to neurodegeneration in Alzheimer's disease and other disorders. Nat. Rev. Neurosci. *12*, 723–738. https://doi.org/10.1038/nrn3114.

75. Kuehner, C. (2017). Why is depression more common among women than among men? Lancet Psychiatry *4*, 146–158. https://doi.org/10.1016/S2215-0366(16)30263-2.

76. Seedat, S., Scott, K.M., Angermeyer, M.C., Berglund, P., Bromet, E.J., Brugha, T.S., Demyttenaere, K., de Girolamo, G., Haro, J.M., Jin, R., et al. (2009). Cross-national associations between gender and mental disorders in the World Health Organization World Mental Health Surveys. Arch. Gen. Psychiatry *66*, 785–795. https://doi.org/10.1001/archgenpsychiatry.2009.36.

77. Abel, K.M., Drake, R., and Goldstein, J.M. (2010). Sex differences in schizophrenia. Int. Rev. Psychiatry *22*, 417–428. https://doi.org/10.3109/09540261.2010.515205.

78. Baldassano, C.F., Marangell, L.B., Gyulai, L., Ghaemi, S.N., Joffe, H., Kim, D.R., Sagduyu, K., Truman, C.J., Wisniewski, S.R., Sachs, G.S., and Cohen, L.S. (2005). Gender differences in bipolar disorder: retrospective data from the first 500 STEP-BD participants. Bipolar Disord. *7*, 465–470. https://doi.org/10.1111/j.1399-5618.2005.00237.x.

79. Rurak, G.M., Woodside, B., Aguilar-Valles, A., and Salmaso, N. (2021). Astroglial cells as neuroendocrine targets in forebrain development: Implications for sex differences in psychiatric disease. Front. Neuroendocrinol. *60*, 100897. https://doi.org/10.1016/j.yfrne.2020.100897.

80. Moreno-Jiménez, E.P., Terreros-Roncal, J., Flor-García, M., Rábano, A., and Llorens-Martín, M. (2021). Evidences for Adult Hippocampal Neurogenesis in Humans. J. Neurosci. *41*, 2541–2553. https://doi.org/10.1523/JNEUROSCI.0675-20.2020.

81. Terreros-Roncal, J., Flor-García, M., Moreno-Jiménez, E.P., Rodríguez-Moreno, C.B., Márquez-Valadez, B., Gallardo-Caballero, M., Rábano, A., and Llorens-Martín, M. (2023). Methods to study adult hippocampal neurogenesis in humans and across the phylogeny. Hippocampus *33*, 271–306. https://doi.org/10.1002/hipo.23474.

82. Schneider, C.A., Rasband, W.S., and Eliceiri, K.W. (2012). NIH Image to ImageJ: 25 years of image analysis. Nat. Methods *9*, 671–675. https://doi.org/10.1038/nmeth.2089.

83. Arganda-Carreras, I., Fernández-González, R., Muñoz-Barrutia, A., and Ortiz-De-Solorzano, C. (2010). 3D reconstruction of histological sections: Application to mammary gland tissue. Microsc. Res. Tech. *73*, 1019–1029. https://doi.org/10.1002/jemt.20829.

84. Virtanen, P., Gommers, R., Oliphant, T.E., Haberland, M., Reddy, T., Cournapeau, D., Burovski, E., Peterson, P., Weckesser, W., Bright, J., et al. (2020). SciPy 1.0: fundamental algorithms for scientific computing in Python. Nat. Methods *17*, 261–272. https://doi.org/10.1038/s41592-019-0686-2.

85. Seabold, S., and Perktold, J. (2010). Statsmodels: Econometric and statistical modeling with python. Proceedings of the 9th Python in Science Conference, 92–96. https://doi.org/10.25080/Majora-92bf1922-011.

86. McKinney, W. (2010). Data Structures for Statistical Computing in Python. Proceedings of the 9th Python in Science Conference, 56–61. https://doi.org/10.25080/Majora-92bf1922-00a.

87. Kim, S., and Webster, M.J. (2019). The Stanley Neuropathology Consortium Integrative Database (SNCID) for Psychiatric Disorders. Neurosci. Bull. *35*, 277–282. https://doi.org/10.1007/s12264-018-0314-7.

88. Torrey, E.F., Webster, M., Knable, M., Johnston, N., and Yolken, R.H. (2000). The stanley foundation brain collection and neuropathology consortium. Schizophr. Res. *44*, 151–155. https://doi.org/10.1016/S0920-9964(99)00192-9.

89. Flor-García, M., Terreros-Roncal, J., Moreno-Jiménez, E.P., Ávila, J., Rábano, A., and Llorens-Martín, M. (2020). Unraveling human adult hippocampal neurogenesis. Nat. Protoc. *15*, 668–693. https://doi.org/10.1038/s41596-019-0267-y.

90. Llorens-Martín, M., Torres-Alemán, I., and Trejo, J.L. (2006). Pronounced individual variation in the response to the stimulatory action of exercise on immature hippocampal neurons. Hippocampus *16*, 480–490. https://doi.org/10.1002/hipo.20175.

91. Rust, R., Kirabali, T., Grönnert, L., Dogancay, B., Limasale, Y.D.P., Meinhardt, A., Werner, C., Laviña, B., Kulic, L., Nitsch, R.M., et al. (2020). A Practical Guide to the Automated Analysis of Vascular Growth, Maturation and Injury in the Brain. Front. Neurosci. *14*, 244. https://doi.org/10.3389/fnins.2020.00244.

Please cite this article in press as: Márquez-Valadez et al., Human adult hippocampal neurogenesis is shaped by neuropsychiatric disorders, demographics, and lifestyle-related factors, Cell Stem Cell (2025), https://doi.org/10.1016/j.stem.2025.08.010

STAR★METHODS

KEY RESOURCES TABLE

REAGENT or RESOURCE	SOURCE	IDENTIFIER
Antibodies		
Rabbit monoclonal anti-Doublecortin (EPR19997) (1:1000)	Abcam	Cat#ab207175; RRID: AB_2894710
Goat polyclonal anti-Doublecortin (1:1000)	Santa Cruz	Cat#sc-8066; RRID: AB_2088494
Mouse monoclonal anti-Polysialylated-neural cell adhesion molecule (PSA-NCAM) (1:1000)	Millipore	Cat#MAB5324; RRID: AB_95211
Rabbit polyclonal anti-Phospho-histone 3 (PH3) (1:250)	Millipore	Cat#06-570; RRID: AB_310177
Rabbit polyclonal anti-Calbindin D28k (CB) (1:2000)	Swant	Cat#CB38a; RRID: AB_2721225
Guinea pig polyclonal anti-S100 calcium-binding protein β (S100β) (1:500)	Synaptic Systems	Cat#287004; RRID: AB_2620025
Chicken polyclonal anti-Vimentin (1:500)	Synaptic Systems	Cat#172006; RRID: AB_2800525
Goat polyclonal anti-SRY (sex determining region Y)-box 2 (Sox2) (1:500)	R and D Systems	Cat# AF2018; RRID: AB_355110
Chicken monoclonal anti-Iba1 (1:500)	Synaptic Systems	Cat# 234 009; RRID: AB_2891282
Mouse monoclonal anti-Phosphorylated γH2A.X (Ser139) (1:500)	Cell signaling Technology	Cat#80312; RRID: AB_2799949
Mouse monoclonal anti-HuC-HuD (1:500)	Thermo Fisher Scientific	Cat#A21271; RRID: AB_221448
Alexa-488 anti-mouse (1:1000)	Thermo Fisher Scientific	Cat#A-21202; RRID: AB_141607
Alexa-488 anti-goat (1:1000)	Thermo Fisher Scientific	Cat#A-11055; RRID: AB_2534102
Alexa-488 anti-chicken (1:1000)	Thermo Fisher Scientific	Cat#A-11039; RRID: AB_2534096
Alexa-555 anti-mouse (1:1000)	Thermo Fisher Scientific	Cat#A-31570; RRID: AB_2536180
Alexa-555 anti-rabbit (1:1000)	Thermo Fisher Scientific	Cat#A-31572; RRID: AB_162543
Alexa-647 anti-mouse (1:1000)	Thermo Fisher Scientific	Cat#A-31571; RRID: AB_162542
Alexa-647 anti-rabbit (1:1000)	Thermo Fisher Scientific	Cat#A-31573; RRID: AB_2536183
Alexa-647 anti-goat (1:1000)	Thermo Fisher Scientific	Cat#A-21447; RRID: AB_2535864
Alexa-647 anti-guinea pig (1:1000)	Thermo Fisher Scientific	Cat#A-21450; RRID: AB_2735091
Biological samples		
Human hippocampal sections obtained from 59 individuals (14 neurologically healthy control subjects, 15 patients with major depression (MD), 15 with schizophrenia (SCH), and 15 with bipolar disorder (BD)	Neuropathology consortium, Stanley Medical Research Institute (SMRI) Brain bank	https://www.stanleyresearch.org/brain-research/neuropathology-consortium/
Chemicals, peptides, and recombinant proteins		
Ulex Europaeus Agglutinin-1 (UEA-1) (1:750)	Vector Laboratories	Cat# B-1065; RRID: AB_2336766
Paraformaldehyde electron microscopy (EM) grade (16% wt/vol)	Electron Microscopy Sciences	Cat#15710
K_2HPO_4	Merck-Millipore	Cat#105101
NaH_2PO_4-H_2O	Merck-Millipore	Cat#567545
Triton X-100	Sigma-Aldrich	Cat#93443
Bovine serum albumin (BSA)	Sigma-Aldrich	Cat#A7888
4 ,6-diamidino-2-phenylindole (DAPI)	Merck-Millipore	Cat#268298
Ethanol (96%)	Merck-Millipore	Cat#159010
Mowiol 4-88	Merck-Millipore	Cat#475904

(*Continued on next page*)

Please cite this article in press as: Márquez-Valadez et al., Human adult hippocampal neurogenesis is shaped by neuropsychiatric disorders, demographics, and lifestyle-related factors, Cell Stem Cell (2025), https://doi.org/10.1016/j.stem.2025.08.010

Continued

REAGENT or RESOURCE	SOURCE	IDENTIFIER
Glycerol (100%)	Sigma-Aldrich	Cat#G9012
Trizma base	Sigma-Aldrich	Cat#T1503
HCl	Merck-Millipore	Cat#113136
Autofluorescence eliminator reagent	Merck-Millipore	Cat#2160
Software and algorithms		
Image J 1.54i	Schneider et al.[82]	https://imagej.nih.gov/ij/
AnalyzeSkeleton ImageJ plugin	Arganda-Carreras et al.[83]	https://imagej.net/plugins/analyze-skeleton/
Graphpad Prism 10.0.3	GraphPad Software, LLC	https://www.graphpad.com/
Jupyter 7.0.6	Jupyter Notebook Contributors	https://jupyter.org/
Python programming language 3.11.7	Python Software Foundation	https://www.python.org/
Scipy module 1.9.3	Virtanen et al.[84]	https://scipy.org/
Statsmodels module 0.14.2	Seabold and Perktold[85]	https://www.statsmodels.org/v0.10.2/#
Pandas module 1.5.3	McKinney[86]	https://pandas.pydata.org/
Other		
ImmEdge Hydrophobic Barrier PAP Pen	Vector Laboratories	Cat#H4000
40 x 50 mm microscopy glass coverslips	Thermo Fisher Scientific	Cat#BC0400050A140MNZ0
LSM 900 Zeiss confocal microscope	Carl Zeiss	https://www.zeiss.com/microscopy/es/home.html
Immersol™ 518 F (Immersion oil)	Carl Zeiss	Cat#444960-0000-000

EXPERIMENTAL MODEL AND STUDY PARTICIPANT DETAILS

A total of 59 participants were included in the present study (14 neurologically healthy control subjects, 15 patients with major depression (MD), 15 with schizophrenia (SCH), and 15 with bipolar disorder (BD)). These subjects (24 females and 35 males) were aged from 25 to 68 y (median: 46 y; mean 45.25 y). Figure S1 provides further demographic data about each subject, including the following: anonymized subject code; clinical diagnosis; age (years); biological sex; post-mortem delay (PMD, namely the time elapsed between *exitus* and sample immersion in fixative) (hours); brain pH; brain weight (g); age at onset of the disease (years); disease duration (years); suicide; psychosis; lifetime dose of fluphenazine or equivalent (mg); consumption of alcohol and drugs of abuse; fixative use; and fixation time. No statistically significant differences in age or PMD were detected between diagnoses (Figures S1B and S1C). This cohort of subjects corresponded to the *Neuropathology consortium* of the Stanley Medical Research Institute (SMRI, USA) Brain Bank.[87,88] Samples were obtained following national laws and international ethical and technical guidelines on the use of human samples for biomedical research purposes. The specimens were collected, processed, and stored in a standardized way (see the STAR Methods section and Figure S2), with informed consent from next-of-kin, by participating medical examiners between September 1993 and June 2005. Brain tissue donation, processing, and use for research complied with published protocols, which include the approval of the whole donation process by the Ethical Committees of the *Instituto de Salud Carlos III* (#CEI PI 30_2020# and #CEI PI 30_2020-V2-Ampliacion 2020#) and the Spanish Research Council (CSIC) (#025/2020# and #198/2020#).

Brain pH was determined using homogenized occipital cortex. Diagnoses were assigned on the basis of clinical examinations by two senior psychiatrists, using DSM-IV criteria and based on medical records and, when necessary, telephone interviews with family members. Diagnoses of unaffected controls were based on structured interviews by a senior psychiatrist with a family member(s) to rule out Axis I diagnoses. Exclusion criteria for all specimens included: I) significant structural brain pathology on post-mortem examination by a qualified neuropathologist; II) history of significant focal neurological signs pre-mortem; III) history of a central nervous system (CNS) disease that could be expected to persistently alter gene expression; IV) documented IQ < 70; and V) poor RNA quality. Additional exclusion criteria for unaffected controls included: I) history of any neurologic or psychiatric disorder, and II) substance abuse within 1 year of death or significant alcohol-related changes in the liver. Brains were screened for the presence of cardiovascular disease, hemorrhage, trauma, tumors, or other pathology and confirmed by the examination of appropriate sections from the suspect area. Cases were also screened for Alzheimer's disease, Parkinson's disease, ethanol-induced changes, and anoxic/hypoxic-related alterations, and also for RNA integrity. Only brains that were free from pathology and that had intact RNA were included in the research cohort. The diagnostic groups and controls were matched for age, sex, race, post-mortem interval (PMI), pH, and the side of the brain frozen.[87,88] Samples were sent and kept coded until all the data analyses were concluded. Moreover, any personal identifying information was anonymized and never disclosed to researchers.

For the alcohol consumption data, subjects were first classified as drinkers/non-drinkers to estimate the effects of alcohol consumption on all the diagnosis groups. Moreover, for those diagnoses in which it was possible (namely they had subjects included

in all the categories), subjects were classified as: non-drinker; social drinker (1-2 drinks/day); moderate drinker in the past (more than 2 drinks per day in the past but not in the present and did not meet criteria for abuse or dependence); current moderate drinker (same as above, in recent months or years); heavy drinker in the past (met criteria for abuse or dependence in the past but not in recent months or years); and current heavy drinker (same as above, in recent months or years). Subjects meeting these criteria for both past and present were coded for present.

METHOD DETAILS

Tissue collection and storage

Tissue was collected by medical examiners following a standardized protocol[88] (Figure S2). Briefly, one hemisphere was cut into 1.5 cm thick coronal slices, frozen in a mixture of isopentane and dry ice, and stored at -70°C. Hippocampi were sectioned at 14 μm thickness with a Leica cryostat. Coded fresh frozen glass-slide-mounted 14μm hippocampal sections were shipped in dry ice.

Tissue fixation

Immediately before immunohistochemistry (IHC), slides were thawed at room temperature (rt) for 10 min. Subsequently, glass-slide-mounted sections were immersed in a 4% paraformaldehyde (PFA) solution for 10 min. The PFA fixative solution (pH = 7.4) was freshly prepared by diluting a commercial 16% PFA solution (Electron Microscopy Sciences) in 0.2 N phosphate buffer (PB) and bi-distilled water (1:2:1). After fixation, samples were washed three times in 0.1 N PB.

Immunohistochemistry

Triple IHC was performed following a previously described protocol[8,9,89] with several modifications adapted to IHC on glass slide-mounted sections. Following tissue fixation (see previous section), an area surrounding each section was drawn using a PAP Pen for Immunostaining (Vector Laboratories) to ensure that the distinct solutions were not split outside that area and to avoid section drying during incubation. Glass slide-mounted sections were then rinsed three times in 0.1 N PB at rt. Subsequently, incubations with primary antibodies (see key resources table) were performed in a humidity chamber at 4°C overnight. Incubation buffer for primary antibodies contained 0.5% Triton X-100 and 0.5% BSA diluted in 0.1 N PB. Following this step, sections were rinsed three times in 0.1 N PB at rt. To detect the binding of primary antibodies, the sections were subsequently incubated with Alexa®-coupled fluorescent secondary antibodies (see key resources table) in a humidity chamber for 2 h at rt. Secondary antibodies were diluted in the same buffer used for primary antibodies. After this incubation, the sections were rinsed 3 times in 0.1 N PB and counterstained for 10 min with DAPI (1:5000) to label nuclei. For Alexa488-*Ulex Europaeus* Agglutinin-I (UEA1) staining, no secondary antibody was used. In this case, sections were incubated with UEA1 in a 0.5% Triton X-100 and 0.5% BSA diluted in 0.1 N PB buffer for the same time as with primary antibodies. In all cases, IHC was followed by a final autofluorescence elimination step. To this end, a commercial Autofluorescence Eliminator reagent (EMD Millipore) was used, following the manufacturer's instructions.[8,9,89] Briefly, the sections were incubated for 2 minutes in 70% ethanol, followed by a 2-minute incubation in an Autofluorescence Eliminator Reagent, then rinsed three times with 70% ethanol and three times with 0.1 N PB. Finally, sections were dried and a non-commercial anti-fading mounting medium (6 g glycerol and 2.4 g mowiol, prepared in 6 ml distilled water and 12 ml 0.2 M Tris-HCl [pH 8.5]) was used to embed and cover the sections. Slides were stored at rt and protected from light in opaque microscope slide cages. To prevent the decay of fluorescent signal intensity and to ensure homogeneity in the time elapsed for all the subjects, confocal images were acquired within two weeks after section mounting. key resources table shows a list of all the chemical reagents used.

Confocal microscopy

Confocal stacks of images were obtained in a LSM900 Zeiss confocal microscope, equipped with three GaAsP detectors. Ten stacks per subject were used to stereologically estimate cell densities and to analyze the vasculature. Depending on the anatomical distribution of cells positive for each marker, stacks were obtained under 63X (Total DGCs, 2 zoom, XY dimensions: 50.7 μm, Z-interval: 1 μm, pinhole dimensions: 0.9 Airy unit), or 40X ($Sox2^+$, $PH3^+$, $vimentin^+$, doublecortin $(DCX)^+$, $HuC\text{-}HuD^+$, $PSA\text{-}NCAM^+$, calbindin $(CB)^+$, $S100\beta^+$, $Iba1^+$, and $\gamma H2AX^+$ cells, and blood vessels and capillaries, 0.68-1.0 zoom, XY dimensions: 234.89-159.72 μm, Z-interval: 1 μm, pinhole dimensions: 0.99 Airy units.) immersion oil objectives, as previously described.[89] For colocalization analyses, 10 stacks per subject were used. To acquire images, the DG was first identified using a 10X dry objective in the DAPI channel. Next, stacks of images were obtained at randomly selected locations. The researchers performing IHC, image acquisition, cell counts, and image analyses were blind to the sex, age, PMD, and diagnoses of the subjects. Two experienced researchers, blind to the aforementioned factors, contributed to the cell counts and vascularization analyses included in this study. They also pooled the data and performed statistical analyses. Demographic data associated with each subject were only disclosed immediately before performing statistical analyses. The SMRI received all the final raw data before disclosing demographic information to the researchers.

Please cite this article in press as: Márquez-Valadez et al., Human adult hippocampal neurogenesis is shaped by neuropsychiatric disorders, demographics, and lifestyle-related factors, Cell Stem Cell (2025), https://doi.org/10.1016/j.stem.2025.08.010

QUANTIFICATION AND STATISTICAL ANALYSIS

Stereological cell counts

Cell densities were estimated by unbiased stereology methods based on the use of the physical dissector method adapted to confocal microscopy.[8,9,89,90] Briefly, two types of cell densities were calculated: total density (encompassing both the granule cell layer (GCL) and the subgranular zone (SGZ)) and local densities (referring to either the GCL or SGZ individually), as presented in the Main and Supplementary Figures. To obtain these measurements, the GCL and SGZ were manually delineated in the DAPI channel of each stack of images using Fiji's freehand drawing tool. The total area was derived by summing the individual areas of the GCL and SGZ, and this was then multiplied by the z-thickness of the stack to calculate the reference volume.[8,89] In the case of the total number of DGCs, the reference volume was determined by multiplying the XY dimensions by the z-thickness of the stack.[89] Next, the cells positive for each marker of interest were counted on individual planes. For each cell type, a z-interval at least 3 times smaller than the average thickness of that particular cell type was selected to allow the tracking of the cell profiles across several planes.[90] The number of positive cells was divided by the corresponding reference volume of each stack of images to calculate cell density (cells/mm^3). Total cell density was estimated by dividing the overall number of positive cells by the combined reference volume of the GCL and SGZ. For local densities, cell counts within each region (GCL or SGZ) were normalized to the respective regional volume (Figure S2). A given cell was considered positive when it showed a clearly and unambiguously identifiable characteristic morphology. Moreover, structures showing signs of apoptosis or nuclear fragmentation on the DAPI channel, or autofluorescence in any of the other three channels, were excluded from cell counts. Depending on the marker of interest, distinct morphological criteria were applied.[9] Vascular structures positive for vimentin were disregarded. Conversely, previously described morphological criteria have been used to identify vimentin$^+$ cells.[9] Colocalization data are presented as the percentage of double-labeled cells out of the total number of cells. However, the signal-to-noise ratio and signal intensity and/or quality were occasionally deemed insufficient to fulfill the strict criteria needed to perform stereological cell counts. In those exceptional cases, individual subjects were excluded from that particular cell count.

Calculation of cell ratios

To estimate cell survival during initial differentiation stages, the density of DCX$^+$ PSA-NCAM$^+$ immature DGCs was divided by that of DCX$^+$ HuC-HuD$^+$ proliferative neuroblasts. To estimate cell survival during the advanced differentiation stages, the density of DCX$^+$ CB$^+$ differentiated DGCs was divided by that of DCX$^+$ PSA-NCAM$^+$ immature DGCs.

Morphometric determinations

To determine cell positioning, the SGZ and the GCL were identified. The SGZ was defined as the 3-cell thickness portion of the GCL adjacent to its hilar border. To determine the area of the nucleus of total DGCs, 50 cells per subject were analyzed. DAPI staining was used to determine the area of the nucleus of DGCs. The nuclear contour was drawn on the plane in which it was maximal, and the area was measured in Fiji. The primary neurites that emerged directly from the soma of DCX$^+$ and DCX$^+$ HuC-HuD$^+$ cells were counted as previously described.[8,9] The percentage of cells with 1, 2, or $\geq$ 3 neurites is shown in the graphs. Finally, to identify the orientation of these neurites, the angle between the hilar border of the GCL and the neurite was measured. A neurite was considered to have an orientation parallel to the SGZ (horizontal neurites) when the angle was $\leq 45^\circ$, whereas it was considered to be vertical when angles ranged between 45° and 90°.[9]

Analysis of the dentate gyrus (DG) vasculature

To determine the area of the DG occupied by blood vessels and capillaries, 10 stacks of confocal images per subject were obtained. Z-stack projections containing an invariant number of planes were obtained and a fixed threshold was applied. The area containing the GCL or the SGZ was traced on the DAPI channel, and the area above the threshold for *Ulex Europeaus* Agglutinin I (UEA-1) was measured and divided by the reference area. To calculate the thickness of capillaries, at least 100 capillaries (50 in the GCL and 50 in the SGZ) per subject were analyzed. Images were zoomed in and a line perpendicular to the trajectory of the vessel was traced.

The vascular skeleton was analyzed following a semi-automated method in Fiji adapted from.[91] Briefly, 90 x 28 μm ROIs of the GCL and SGZ were obtained from each Z-stack projection. Subsequently, a threshold was applied and small artifacts were removed before image binarization. The total vascular length, branches, and junctions were traced using the Skeleton plugin from *Fiji*, and measures were normalized by the reference area. The tortuosity index was calculated as the branch length divided by the Euclidean distance (length of the line segment between the beginning and the end of the branch), minus 1 to account for the difference.

Statistical analyses

Statistical analyses were performed using GraphPad 10 software. Outlier values were identified by the ROUT method. Extreme outlier values are not shown in the graphs and were excluded from statistical comparisons. The Kolmogorov-Smirnov normality test was used to check the normality of sample distribution. In those cases in which the effect of a single variable was analyzed, the data were compared using the Student t-test/Mann-Whitney U-test or one-way ANOVA tests. To compare the effect of more than one variable, a two-way ANOVA test was used. In those cases in which the one- or two-way ANOVA test was statistically significant

Please cite this article in press as: Márquez-Valadez et al., Human adult hippocampal neurogenesis is shaped by neuropsychiatric disorders, demographics, and lifestyle-related factors, Cell Stem Cell (2025), https://doi.org/10.1016/j.stem.2025.08.010

and there were more than two levels, Tukey's Honestly Significant Difference (HSD) multiple comparison post-hoc analyses were used to compare the differences between individual groups. In those cases, asterisks on the graphs indicate the results of post-hoc comparisons. A two-sided Pearson s correlation test was applied to determine correlations between experimental variables. All graphs represent mean values ± SEM. A 95% confidence interval was used for statistical comparisons. Data S1 file shows the detailed results of the statistical comparisons. Table S1 includes Raw data.

To stratify data by biological sex, suicide, psychosis, treatment with antipsychotic drugs, or consumption of alcohol or drugs of abuse, statistical analyses were performed in batches using Python software. In this case, outliers were identified by the interquartile range (IQR) method, and extreme values were excluded. The subsequent statistical analyses were performed as described above.

Cell Stem Cell, Volume *32*

Supplemental Information

Human adult hippocampal neurogenesis is shaped by neuropsychiatric disorders, demographics, and lifestyle-related factors

Berenice Márquez-Valadez, Marta Gallardo-Caballero, and María Llorens-Martín

Supplementary Figure S1. Demographic data. A: Epidemiological data of the subjects included in this study. The subject code, clinical diagnosis, age, sex, post-mortem delay (PMD, i.e., the time lapse between *exitus* and tissue immersion in fixative), brain pH, brain weight (g), age at onset of the disease, duration (years), suicide (yes/no), psychosis (yes/no), consumption of drugs of abuse (yes/no), consumption of alcohol (yes/no), and the fixation time and fixative used are indicated. **B**: Age of the subjects included in this study. **C**: PMD of the samples used in this study. S: Social drinker (1–2 drinks/day). M: Moderate drinker (>2 drinks/day). H: Heavy drinker (met criteria for abuse or dependence). Present: Pr. Past: P. Graphs represent mean values ± SEM. Results from statistical comparisons are detailed in **Data S1**.

Related to Figures 1 – 7.

A

Subject	Clinical diagnose	Age (years)	Sex	PMD (h)	Brain pH	Brain weight (gr)	Onset (years)	Duration (years)	Suicide	Psychosis	Substance consumption	Alcohol consumption	Fixative
Control 1	Control	52	Male	28	6.5	1700	0	0	No	No	No	Yes (M, P)	4% PFA, 10 min
Control 2	Control	44	Female	25	6.3	1490	0	0	No	No	No	Yes (S)	4% PFA, 10 min
Control 3	Control	59	Male	26	6.4	1560	0	0	No	No	No	Yes (M, Pr)	4% PFA, 10 min
Control 4	Control	52	Male	8	6.5	1840	0	0	No	No	No	Yes (S)	4% PFA, 10 min
Control 5	Control	53	Male	28	6.2	1400	0	0	No	No	Yes	Yes (M, P)	4% PFA, 10 min
Control 6	Control	44	Male	10	6.4	1510	0	0	No	No	No	Yes (S)	4% PFA, 10 min
Control 7	Control	35	Female	23	6.6	1340	0	0	No	No	No	Yes (S)	4% PFA, 10 min
Control 8	Control	41	Male	11	6	1305	0	0	No	No	No	Yes (S)	4% PFA, 10 min
Control 9	Control	42	Male	27	6.6	1500	0	0	No	No	No	No	4% PFA, 10 min
Control 10	Control	35	Female	40	5.8	1560	0	0	No	No	No	No	4% PFA, 10 min
Control 11	Control	68	Female	13	6.3	1360	0	0	No	No	No	No	4% PFA, 10 min
Control 12	Control	58	Male	27	6	1780	0	0	No	No	No	Yes (S)	4% PFA, 10 min
Control 13	Control	29	Female	42	6.2	1440	0	0	No	No	No	No	4% PFA, 10 min
Control 14	Control	57	Female	26	6	1400	0	0	No	No	No	No	4% PFA, 10 min
MD 1	Major depression	32	Female	47	6	1500	32	1	Yes	No	Yes	No	4% PFA, 10 min
MD 2	Major depression	53	Female	40	6.3	1320	11	42	No	No	No data	Yes (H, Pr)	4% PFA, 10 min
MD 3	Major depression	44	Female	32	6.2	1410	27	17	Yes	No	No	Yes (S)	4% PFA, 10 min
MD 4	Major depression	65	Male	19	6.2	1360	45	20	No	No	No	Yes (S)	4% PFA, 10 min
MD 5	Major depression	52	Male	12	6.5	1520	46	6	No	No	No	Yes (S)	4% PFA, 10 min
MD 6	Major depression	46	Male	26	6.1	1720	28	18	Yes	No	No	No	4% PFA, 10 min
MD 7	Major depression	42	Female	25	6.3	1340	39	3	No	No	No	Yes (S)	4% PFA, 10 min
MD 8	Major depression	51	Male	26	6.3	1550	50	1	Yes	No	No	Yes (H, P)	4% PFA, 10 min
MD 9	Major depression	39	Male	23	6	1530	17	22	Yes	No	Yes	Yes (H, Pr)	4% PFA, 10 min
MD 10	Major depression	42	Male	7	6.2	1350	32	10	Yes	No	Yes	No	4% PFA, 10 min
MD 11	Major depression	56	Male	23	6.5	1240	52	4	No	No	No	No	4% PFA, 10 min
MD 12	Major depression	56	Female	28	5.8	1520	54	2	No	No	No	Yes (S)	4% PFA, 10 min
MD 13	Major depression	30	Female	33	6	1370	19	11	Yes	No	No	Yes (M, Pr)	4% PFA, 10 min
MD 14	Major depression	43	Male	43	5.9	1460	30	13	No	No	Yes	Yes (H, Pr)	4% PFA, 10 min
MD 15	Major depression	47	Male	28	6.4	1740	27	20	No	No	No	No	4% PFA, 10 min
SCH 1	Schizophrenia	30	Female	60	6.2	1430	22	8	Yes	Yes	Yes	Yes (M, P)	4% PFA, 10 min
SCH 2	Schizophrenia	52	Male	61	6	1530	20	32	No	Yes	No	No	4% PFA, 10 min
SCH 3	Schizophrenia	30	Male	32	5.8	1620	13	17	No	Yes	No	Yes (S)	4% PFA, 10 min
SCH 4	Schizophrenia	62	Female	26	6.1	1270	38	24	No	Yes	No	Yes (S)	4% PFA, 10 min
SCH 5	Schizophrenia	60	Female	40	6.2	1395	15	45	No	Yes	No	No	4% PFA, 10 min
SCH 6	Schizophrenia	60	Male	31	6.2	1340	27	33	No	Yes	No	No	4% PFA, 10 min
SCH 7	Schizophrenia	32	Male	19	6.1	1590	27	5	No	Yes	Yes	Yes (H, Pr)	4% PFA, 10 min
SCH 8	Schizophrenia	31	Male	14	5.8	1555	18	13	Yes	Yes	No	Yes (S)	4% PFA, 10 min
SCH 9	Schizophrenia	58	Female	26	5.9	1410	42	16	No	Yes	No	Yes (H, P)	4% PFA, 10 min
SCH 10	Schizophrenia	25	Male	32	6.6	1555	20	5	Yes	Yes	No	Yes (H, P)	4% PFA, 10 min
SCH 11	Schizophrenia	44	Male	50	6.5	1640	17	27	No	Yes	No	Yes (M, Pr)	4% PFA, 10 min
SCH 12	Schizophrenia	44	Male	29	5.9	1500	21	23	No	Yes	Yes	Yes (M, P)	4% PFA, 10 min
SCH 13	Schizophrenia	56	Female	12	6.4	1420	24	32	Yes	Yes	Yes	No	4% PFA, 10 min
SCH 14	Schizophrenia	35	Male	35	6.5	1380	19	16	No	Yes	Yes	Yes (M, Pr)	4% PFA, 10 min
SCH 15	Schizophrenia	49	Female	38	6.2	1440	25	24	No	Yes	No	No	4% PFA, 10 min
BD 1	Bipolar disorder	25	Female	24	6.4	1540	19	6	Yes	Yes	Yes	Yes (H, Pr)	4% PFA, 10 min
BD 2	Bipolar disorder	48	Female	22	5.8	1260	16	32	No	Yes	Yes	Yes (H, Pr)	4% PFA, 10 min
BD 3	Bipolar disorder	37	Female	29	6.5	1130	14	23	Yes	Yes	Yes	Yes (S)	4% PFA, 10 min
BD 4	Bipolar disorder	54	Male	39	5.8	1690	39	14	No	No	No	Yes (H, P)	4% PFA, 10 min
BD 5	Bipolar disorder	30	Male	31	6.1	1350	22	8	No	Yes	No	Yes (M, Pr)	4% PFA, 10 min
BD 6	Bipolar disorder	30	Male	56	5.8	1580	7	23	Yes	No	No	Yes (S)	4% PFA, 10 min
BD 7	Bipolar disorder	57	Male	19	6.2	1440	30	27	No	Yes	No	Yes (H, P)	4% PFA, 10 min
BD 8	Bipolar disorder	34	Male	23	6.3	1523	19	15	Yes	Yes	Yes	Yes (H, Pr)	4% PFA, 10 min
BD 9	Bipolar disorder	48	Male	13	6.1	1540	27	21	Yes	Yes	Yes	Yes (M, P)	4% PFA, 10 min
BD 10	Bipolar disorder	31	Male	28	6.3	1680	21	10	Yes	Yes	Yes	Yes (H, P)	4% PFA, 10 min
BD 11	Bipolar disorder	30	Male	45	6.3	1590	14	16	Yes	No	Yes	No	4% PFA, 10 min
BD 12	Bipolar disorder	50	Female	18	6.1	1180	34	16	No	Yes	Yes	Yes (M, Pr)	4% PFA, 10 min
BD 13	Bipolar disorder	61	Female	60	6.5	1415	18	43	Yes	Yes	No	Yes (S)	4% PFA, 10 min
BD 14	Bipolar disorder	50	Male	19	6.2	1380	17	23	Yes	Yes	No	Yes (S)	4% PFA, 10 min
BD 15	Bipolar disorder	50	Female	62	6.3	1320	25	25	No	No	No	No	4% PFA, 10 min

B

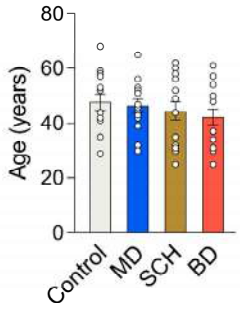

C

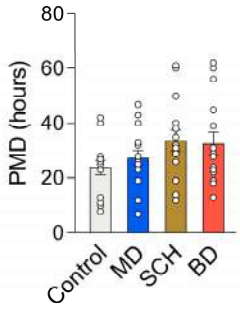

Supplementary Figure S2. Experimental design. Post-mortem human brain tissue was collected and hippocampal fragments were frozen to obtain 14 μm thick sections using a Leica cryostat. Sections were mounted on glass slides and stored at -70ºC (tissue collection – top panel). Prior to immunohistochemistry (IHC) detection, glass slide-mounted sections were fixed in a freshly prepared solution of 4% paraformaldehyde (PFA) for 10 min. Subsequently, tissue delineation and antibody incubation were performed, followed by a final step of autofluorescence elimination (tissue processing – middle panel). Confocal stacks of images were obtained in an LSM900 Zeiss confocal microscope (10 stacks per subject). The stereological cell counts, morphometric characterizations, and vasculature analyses were performed in the same stacks. Finally, GraphPad 10 software was used for statistical analyses (data collection and analysis – bottom panel).

Related to Figures 1 – 7.

Tissue collection

Brain collection

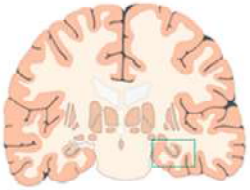

Hippocampal dissection

Cryo-sectioning

-70°C storage

Tissue processing

Defrosting

Fixation

Delineation

Antibody incubation

Autofluorescence elimination

Data collection

Confocal microscope image acquisition

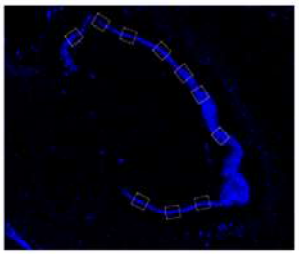

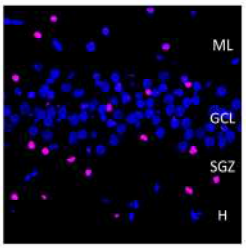

Stereological quantification

Total densities

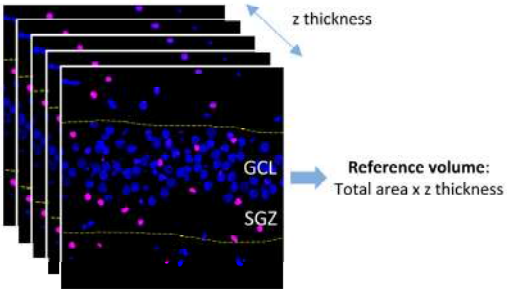

Local densities

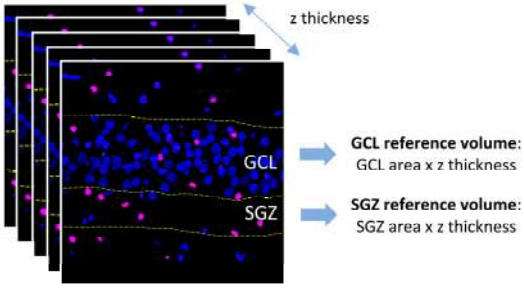

$$\textbf{Cell density (cells / mm3)} = \frac{\text{n}^{\text{o}}\text{ cells inside reference volume}}{\text{reference volume (mm}^3\text{)}}$$

Supplementary Figure S3. Supplementary data obtained from neurologically healthy control subjects and patients with major depression (MD). A: Total and local density of subgranular zone (SGZ) and granule cell layer (GCL) doublecortin $(DCX)^+$ immature dentate granule cells (DGCs), and total density of DCX^+ HuC-HuD^+, DCX^+ polysialylated-neural cell adhesion molecule $(PSA\text{-}NCAM)^+$, and DCX^+ calbindin $(CB)^+$ cells. **B:** ratio of DCX^+ $PSA\text{-}NCAM^+$ early differentiating immature DGCs to DCX^+ HuC-HuD^+ proliferative neuroblasts. **C:** ratio of DCX^+ CB^+ late-differentiating immature DGCs to DCX^+ $PSA\text{-}NCAM^+$ early-differentiating immature DGCs. **D:** Percentage of phospho-histone 3 $(PH3)^+$ cells that express S100 calcium-binding protein B (S100β). **E:** Area of the nucleus of DGCs. **F – O:** Location of SRY (sex-determining region Y)-box 2 $(Sox2)^+$ (**F**), $vimentin^+$ $PH3^+$ $S100\beta^-$ (**G**), $PH3^+$ (**H**), DCX^+ HuC-HuD^+ (**I**), PSA-$NCAM^+$ (**J**), DCX^+ $PSA\text{-}NCAM^+$ (**K**), DCX^+ CB^+ (**L**), $S100\beta^+$ (**M**), $Iba1^+$ (**N**), and phosphorylated H2AX $(\gamma H2AX)^+$ (**O**) cells. **P – Q:** Number (**P**) and orientation (**Q**) of neurites in DCX^+ HuC-HuD^+ cells. n = 14 neurologically healthy control subjects and 15 patients with MD. In **C**, Z-projection images are shown. Graphs represent mean values ± SEM. * $0.05 > p \geq 0.01$; ** $0.01 > p \geq 0.001$; *** $p < 0.001$. Detailed results of statistical comparisons are shown in **Data S1**.

Related to Figures 3 and **4**.

Supplementary data. Adult hippocampal neurogenesis in patients with major depression.

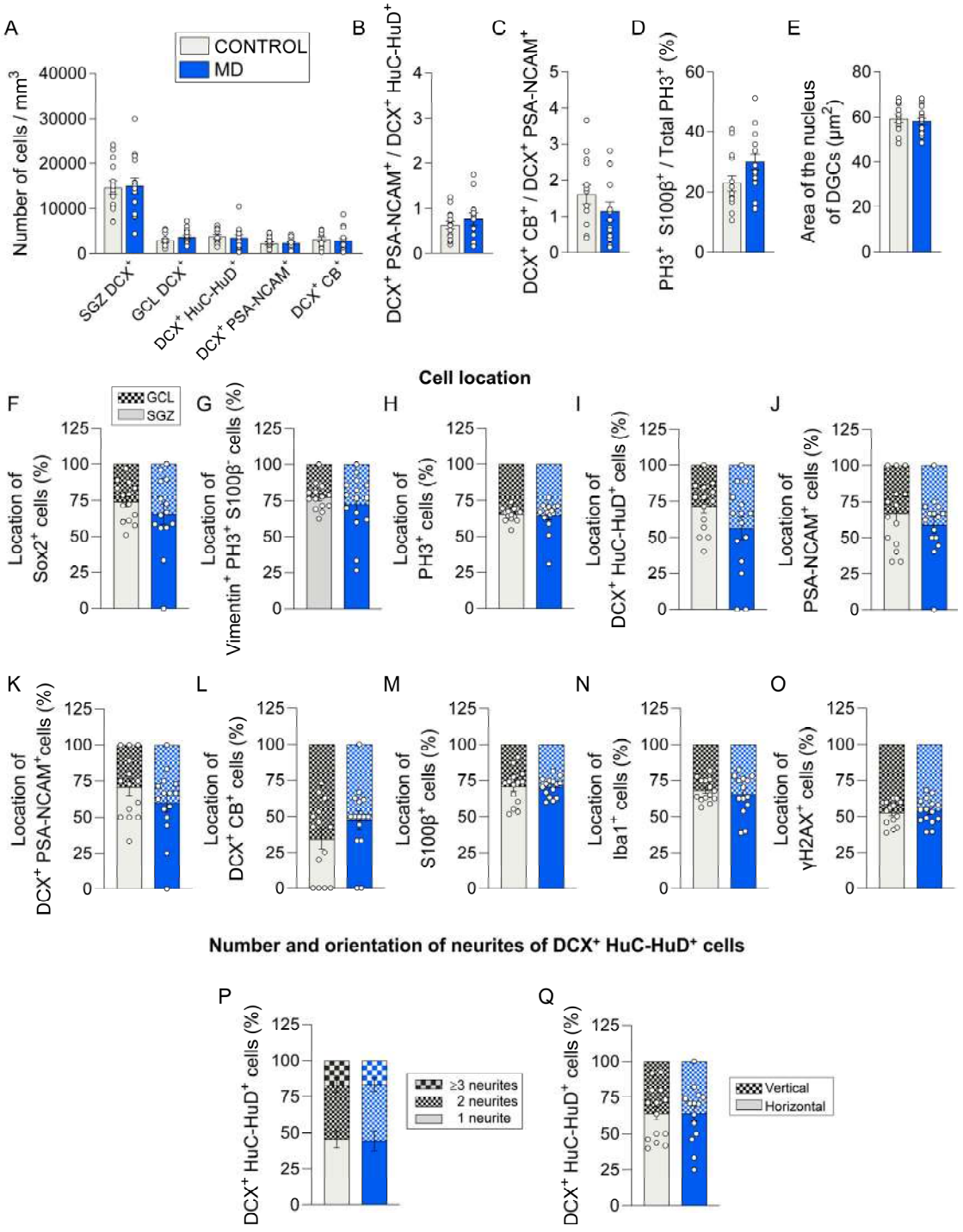

Supplementary Figure S4. Vascularization in neurologically healthy control subjects and patients with major depression (MD). A – E: Area occupied by (**A**), thickness (**B**), normalized length (**C**), and number of branches (**D**) and junctions (**E**) of *Ulex Europaeus* Agglutinin-I $(UEA1)^+$ capillaries in the subgranular zone (SGZ). **F – K:** Area occupied by (**F**), thickness (**G**), normalized length (**H**), tortuosity index (**I**), and number of branches (**J**) and junctions (**K**) of $UEA1^+$ capillaries in the granule cell layer (GCL). **L – P:** Area occupied by (**L**), thickness (**M**), normalized length (**N**), and number of branches (**O**) and junctions (**P**) of total (GCL + SGZ) $UEA1^+$ capillaries. **Q:** Normalized ratio of the SGZ/GCL area occupied by $UEA1^+$ capillaries. **R:** SGZ/GCL capillary thickness ratio. n = 14 neurologically healthy control subjects and 15 patients with MD. Graphs represent mean values ± SEM. Detailed results of statistical comparisons are shown in **Data S1**.

Related to Figures 3 and **4**.

Supplementary data. Dentate gyrus vascularization in neurologically healthy control subjects and patients with major depression (MD).

Vascularization in the subgranular zone (SGZ).

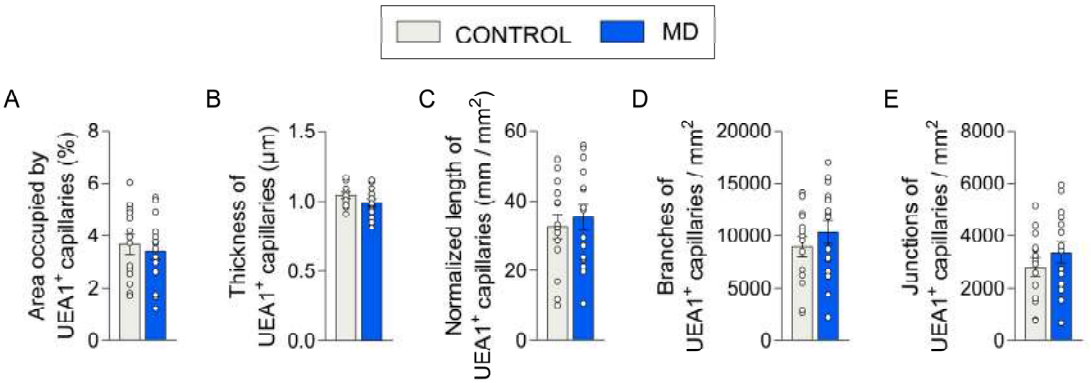

Vascularization in the granule cell layer (GCL).

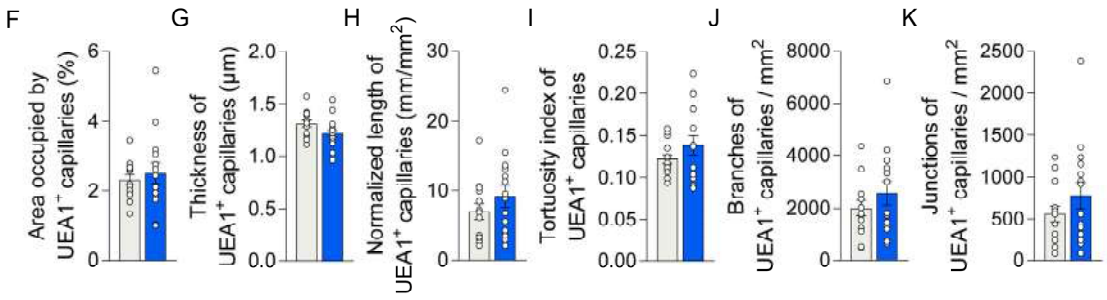

Vascularization in the dentate gyrus (SGZ + GCL).

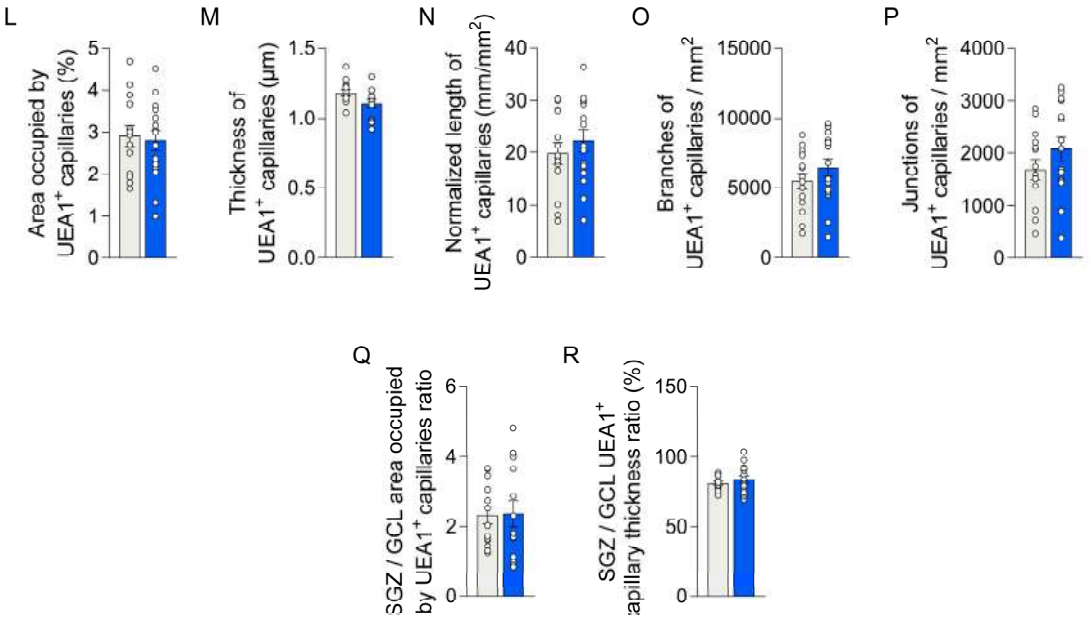

Supplementary Figure S5. Supplementary data obtained from patients with major depression (MD). A: Statistically significant correlation between the age of the subject and the density of vimentin^{+} phospho-histone 3 (PH3)$^{+}$ S100 calcium-binding protein B (S100β)$^{-}$ proliferative neural stem cells (NSCs) in the subgranular zone (SGZ). **B – D:** Statistically significant correlations between the duration of the disease and the subgranular zone (SGZ) area occupied by (**B**), and the thickness of total (**C**) and granule cell layer (GCL) (**D**) *Ulex Europaeus* Agglutinin-I (UEA1)$^{+}$ capillaries. **E – F:** Statistically significant correlations between the onset of the disease and the density of Iba1^{+} microglia (**E**), and the area of the SGZ occupied by UEA1^{+} capillaries (**F**). **G – O:** Statistically significant comparisons of data obtained from patients with MD stratified by biological sex (**G – H**), suicide (**I**), and consumption of alcohol (**J – O**). **G:** Orientation of neurites in DCX^{+} HuC-HuD^{+} cells. **H:** SGZ/GCL *Ulex Europaeus* Agglutinin-I (UEA1)$^{+}$ capillary thickness ratio. **I:** Tortuosity index of GCL UEA1^{+} capillaries. **J – K:** Density (**J**) and location (**K**) of SRY (sex-determining region Y)-box 2 (Sox2)$^{+}$ cells. **L:** Percentage of DCX+ cells that express HuC-HuD. **M:** Density of Iba1^{+} cells. **N:** Location of phosphorylated H2AX (γH2AX). **O:** Normalized ratio of the SGZ/GCL area occupied by UEA1^{+} capillaries. n = 15 patients with MD. Graphs represent mean values ± SEM. * $0.05 > p \geq 0.01$; ** $0.01 > p \geq 0.001$; *** $p < 0.001$. Detailed results of statistical comparisons are shown in **Data S1**.

Related to Figures 3 and **4**.

Supplementary data.
Statistically significant comparisons of data obtained from patients with major depression (MD).
Correlations between cell densities/vascularization and the age, disease duration and disease onset.

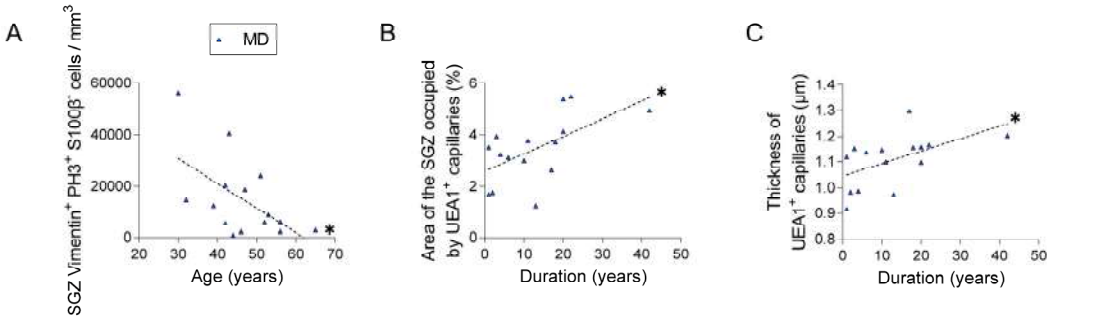

Data stratified by biological sex (F: Female; M: Male).

Data stratified by suicide.

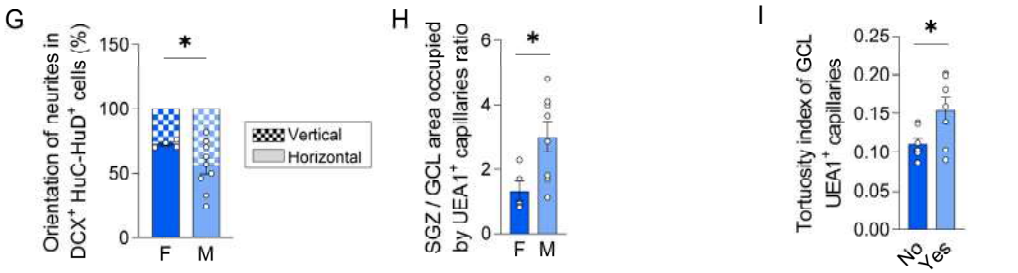

Data stratified by alcohol consumption.

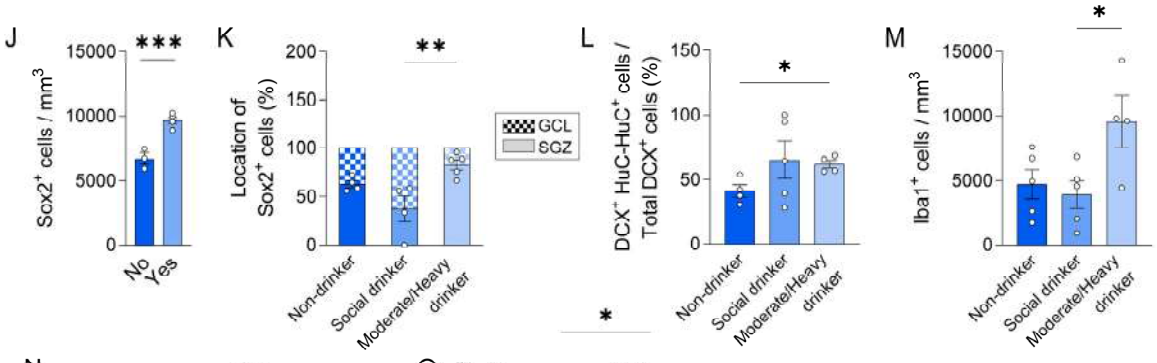

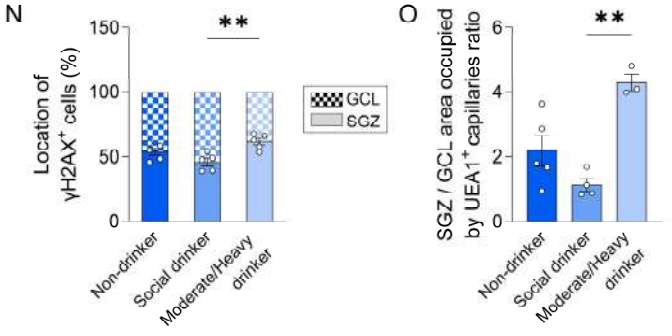

Supplementary Figure S6. Supplementary data obtained from neurologically healthy control subjects and patients with schizophrenia (SCH). A: Total and local density of subgranular zone (SGZ) and granule cell layer (GCL) doublecortin $(DCX)^+$ immature dentate granule cells (DGCs), and total density of DCX^+ HuC-HuD^+, DCX^+ polysialylated-neural cell adhesion molecule $(PSA\text{-}NCAM)^+$, and DCX^+ calbindin $(CB)^+$ cells. **B:** ratio of DCX^+ $PSA\text{-}NCAM^+$ early differentiating immature DGCs to DCX^+ HuC-HuD^+ proliferative neuroblasts. **C:** ratio of DCX^+ CB^+ late-differentiating immature DGCs to DCX^+ $PSA\text{-}NCAM^+$ early-differentiating immature DGCs. **D:** Percentage of phospho-histone 3 $(PH3)^+$ cells that express S100 calcium-binding protein B (S100β). **E:** Area of the nucleus of DGCs. **F – O:** Location of SRY (sex-determining region Y)-box 2 $(Sox2)^+$ (**F**), $vimentin^+$ $PH3^+$ $S100\beta^-$ (**G**), $PH3^+$ (**H**), DCX^+ HuC-HuD^+ (**I**), PSA-$NCAM^+$ (**J**), DCX^+ $PSA\text{-}NCAM^+$ (**K**), DCX^+ CB^+ (**L**), $S100\beta^+$ (**M**), $Iba1^+$ (**N**), and phosphorylated H2AX $(\gamma H2AX)^+$ (**O**) cells. **P – Q:** Number (**P**) and orientation (**Q**) of neurites in DCX^+ HuC-HuD^+ cells. n = 14 neurologically healthy control subjects and 15 patients with SCH. In **C**, Z-projection images are shown. Graphs represent mean values ± SEM. * $0.05 > p \geq 0.01$; ** $0.01 > p \geq 0.001$. Detailed results of statistical comparisons are shown in **Data S1**.

Related to Figure 5.

Supplementary data. Adult hippocampal neurogenesis in patients with schizophrenia (SCH)

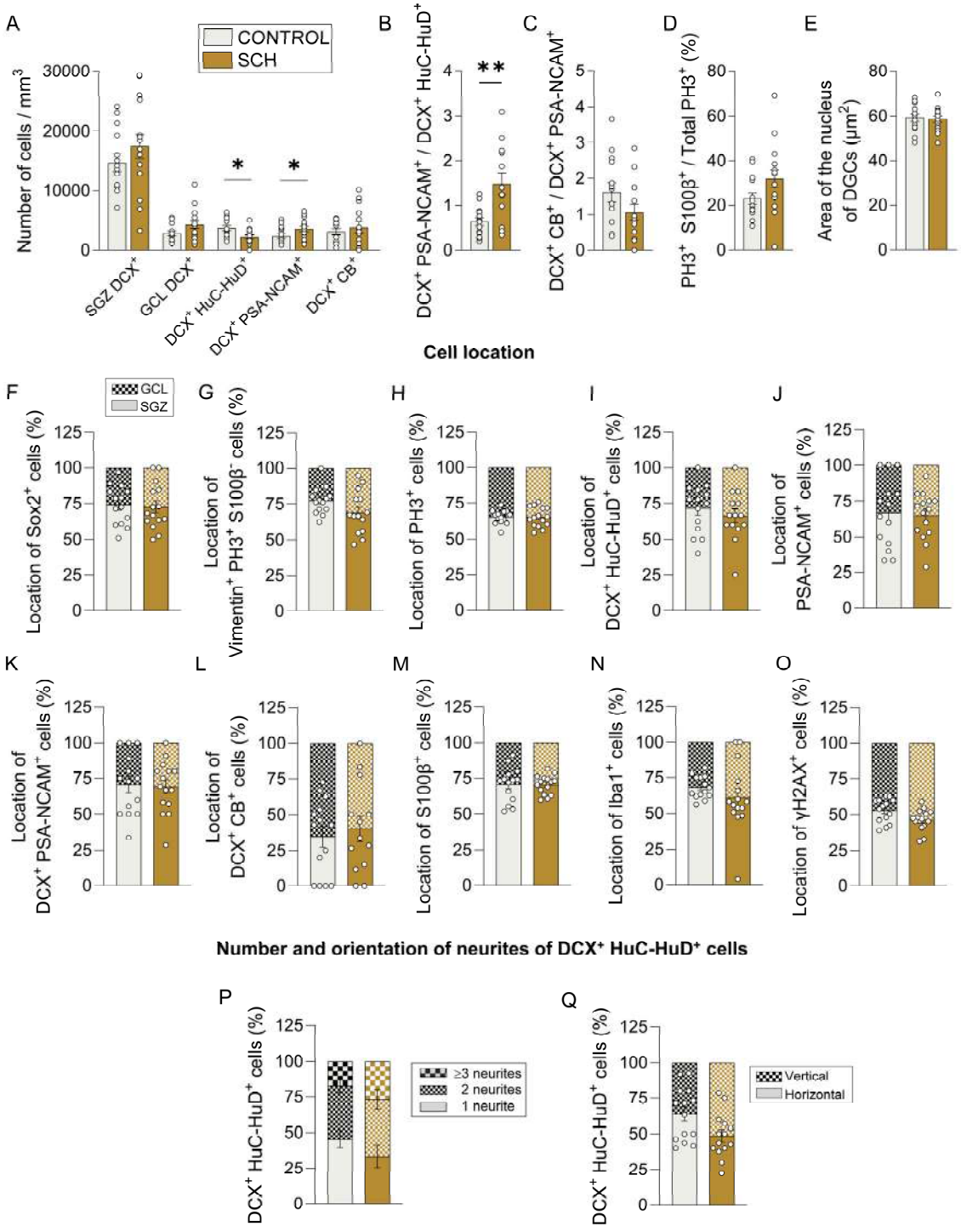

Supplementary Figure S7. Vascularization in neurologically healthy control subjects and patients with schizophrenia (SCH). A – F: Area occupied by (**A**), thickness (**B**), normalized length (**C**), tortuosity index (**D**), and number of branches (**E**) and junctions (**F**) of *Ulex Europaeus* Agglutinin-I $(UEA1)^+$ capillaries in the subgranular zone (SGZ). **G – L:** Area occupied by (**G**), thickness (**H**), normalized length (**I**), tortuosity index (**J**), and number of branches (**K**) and junctions (**L**), and of $UEA1^+$ capillaries in the granule cell layer (GCL). **M – R:** Area occupied by (**M**), thickness (**N**), normalized length (**O**), tortuosity index (**P**), and number of branches (**Q**) and junctions (**R**) of total (GCL + SGZ) $UEA1^+$ capillaries. **S:** SGZ/GCL $UEA1^+$ capillary thickness ratio. n = 14 neurologically healthy control subjects and 15 patients with SCH. Graphs represent mean values ± SEM. Detailed results of statistical comparisons are shown in **Data S1**.

Related to Figure 5.

Supplementary data. Dentate gyrus vascularization in neurologically healthy control subjects and patients with schizophrenia (SCH).

Vascularization in the subgranular zone (SGZ).

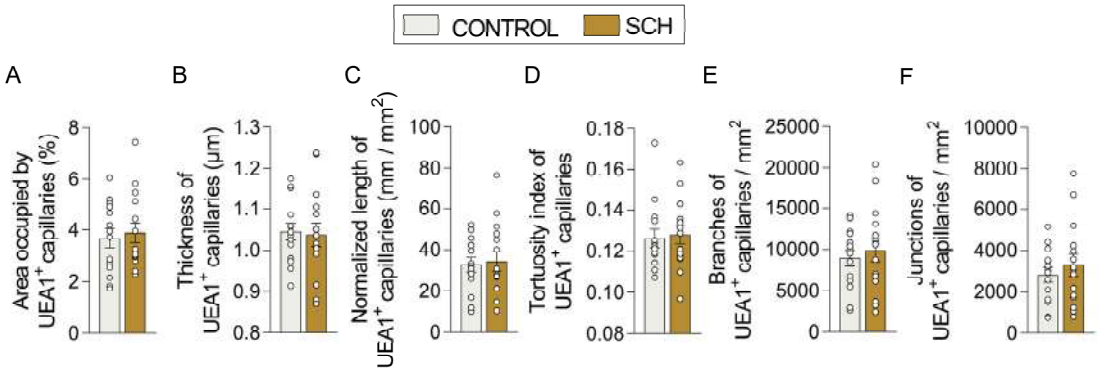

Vascularization in the granule cell layer (GCL).

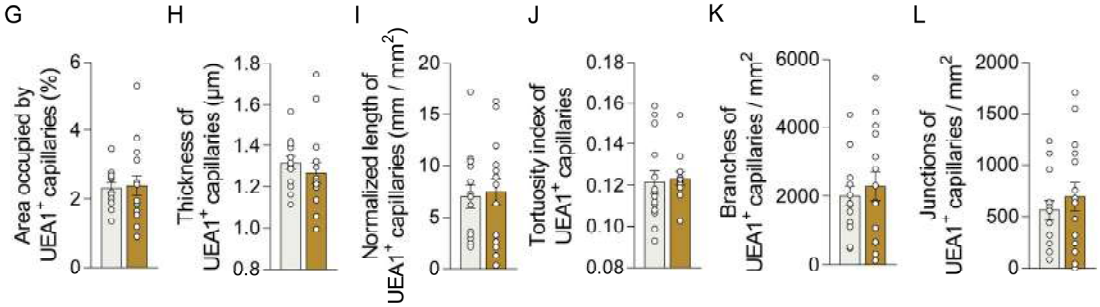

Vascularization in the dentate gyrus (SGZ+GCL).

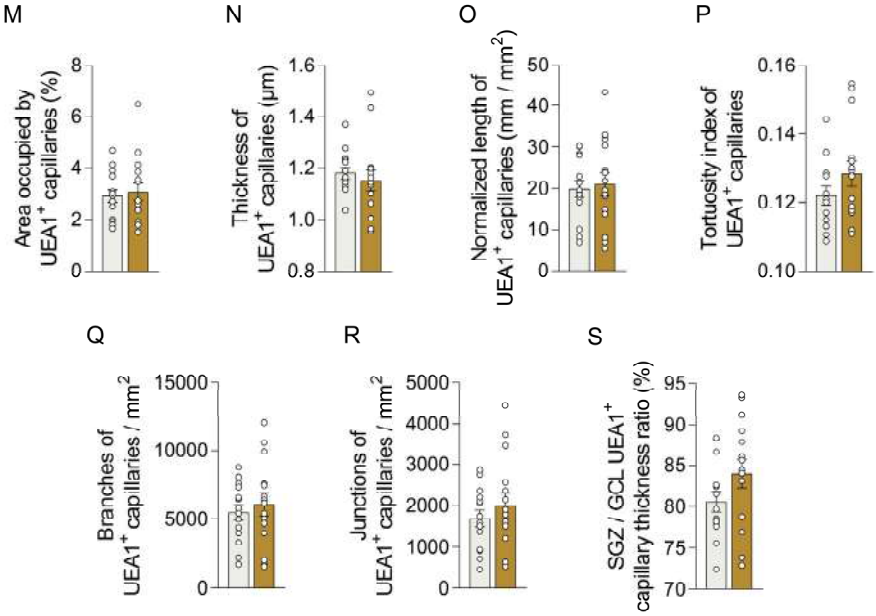

Supplementary Figure S8. Supplementary data obtained from patients with schizophrenia (SCH). A – G: Statistically significant correlations between the age of the subject and the area occupied by *Ulex Europaeus* Agglutinin-I $(UEA1)^+$ capillaries in the subgranular zone (SGZ) (**A**) and the granule cell layer (GCL) (**B**), thickness (**C**), normalized length (**D**), and number of branches (**E**) and junctions (**F**) of GCL $UEA1^+$ capillaries, and normalized ratio of the SGZ/ GCL area occupied by $UEA1^+$ capillaries (**G**). **H – S:** Statistically significant correlations between the duration of the disease and the total (**H**), SGZ (**I**), and GCL (**J**) area occupied by $UEA1^+$ capillaries, total (**K**) and GCL (**L**) normalized length of $UEA1^+$ capillaries, total (**M**), SGZ (**N**), and GCL (**O**) number of branches of $UEA1^+$ capillaries, total (**P**), SGZ (**Q**), and GCL (**R**) junctions of $UEA1^+$ capillaries, and SGZ/GCL $UEA1^+$ capillary thickness ratio (**S**). **T:** Statistically significant correlations between the age at onset of the disease and the density of $vimentin^+$ phospho-histone 3 $(PH3)^+$ S100 calcium-binding protein B $(S100\beta)^-$ proliferative neural stem cells in the GCL. **U – AF:** Statistically significant comparisons of data obtained from patients with SCH stratified by suicide (**U – AA**), treatment with anti-psychotic drugs (patients were stratified depending on whether they received a lifetime dose of fluphenazine or equivalent of more or less than 5000 mg) (**AB – AD**), and alcohol consumption (**AE - AF**). **U – V:** Orientation of neurites in DCX^+ immature DGCs (**U**) and DCX^+ HuC-HuD proliferative neuroblasts (**V**). **W – Y:** Total (GCL + SGZ) (**W**), SGZ (**X**), and GCL (**Y**) area occupied by *Ulex Europaeus* Agglutinin-I $(UEA1)^+$ capillaries. **Z:** Tortuosity index of GCL $UEA1^+$ capillaries. **AA:** Normalized ratio of the SGZ/GCL area occupied by $UEA1^+$ capillaries. **AB:** Density of DGCs. **AC:** Location of $PH3^+$ cells. **AD:** Density of $vimentin^+$ $S100\beta^-$ neural stem cells. **AE:** Location of $Iba1^+$ cells. **AF:** Thickness of $UEA1^+$ capillaries in the SGZ. n = 15 patients with SCH. Graphs represent mean values ± SEM. * $0.05 > p \geq 0.01$; ** $0.01 > p \geq 0.001$. Detailed results of statistical comparisons are shown in **Data S1**.

Related to Figure 5.

Supplementary data.
Statistically significant comparisons of data obtained from patients with schizophrenia (SCH).
Correlations between cell densities/vascularization and the age, disease duration and disease onset.

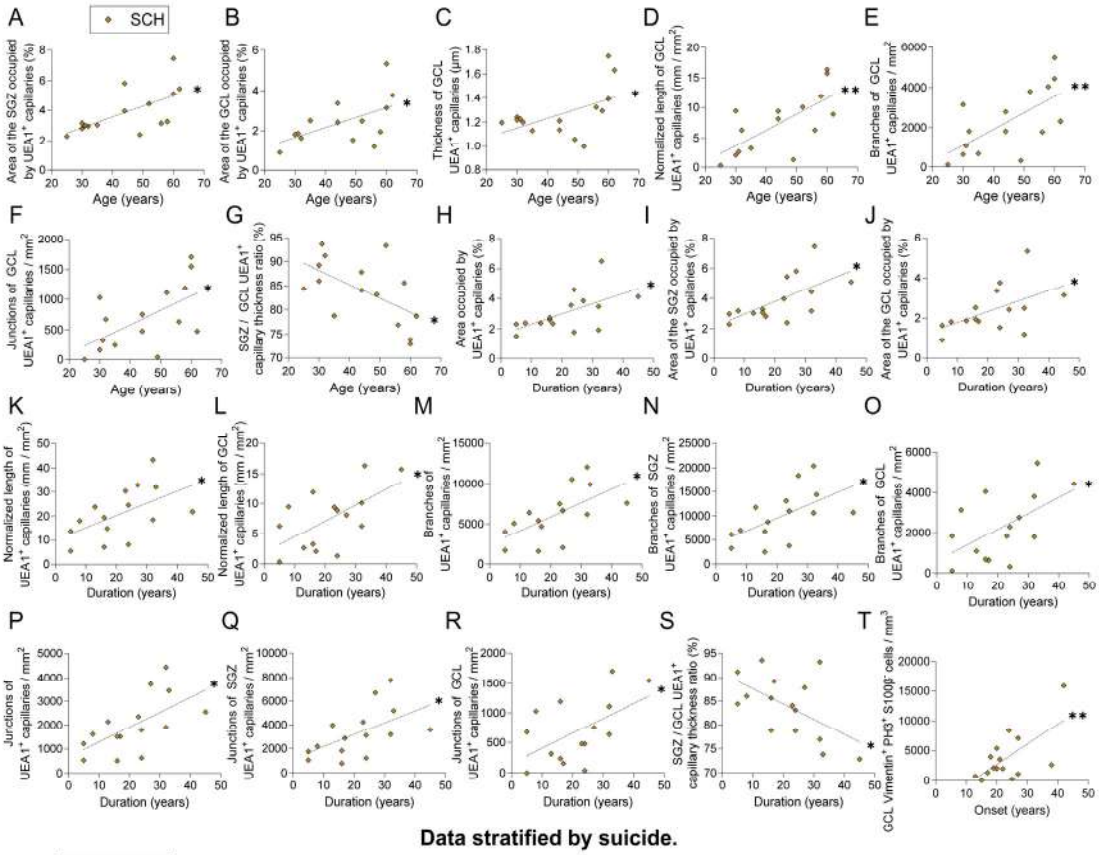

Data stratified by suicide.

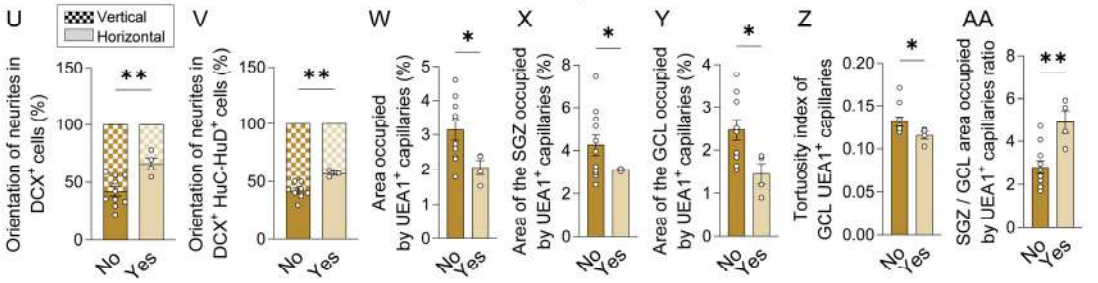

Data stratified by antipsychotic treatment.

Data stratified by alcohol consumption.

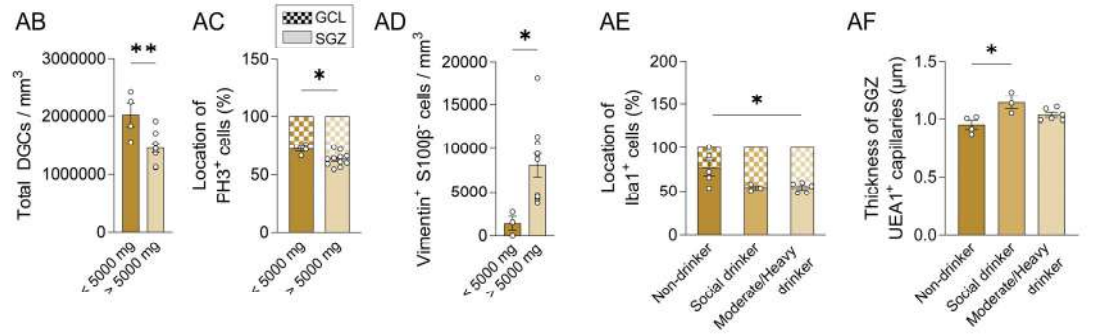

Supplementary Figure S9. Supplementary data obtained from neurologically healthy control subjects and patients with bipolar disorder (BD). A: Total and local density of subgranular zone (SGZ) and granule cell layer (GCL) doublecortin $(DCX)^+$ immature dentate granule cells (DGCs), and total density of DCX^+ HuC-HuD^+, DCX^+ polysialylated-neural cell adhesion molecule $(PSA\text{-}NCAM)^+$, and DCX^+ calbindin $(CB)^+$ cells. **B:** ratio of DCX^+ $PSA\text{-}NCAM^+$ early differentiating immature DGCs to DCX^+ HuC-HuD^+ proliferative neuroblasts. **C:** ratio of DCX^+ CB^+ late-differentiating immature DGCs to DCX^+ $PSA\text{-}NCAM^+$ early-differentiating immature DGCs. **D:** Percentage of phospho-histone 3 $(PH3)^+$ cells that express S100 calcium-binding protein B (S100β). **E:** Area of the nucleus of DGCs. **F – O:** Location of SRY (sex-determining region Y)-box 2 $(Sox2)^+$ (**F**), $vimentin^+$ $PH3^+$ $S100\beta^-$ (**G**), $PH3^+$ (**H**), DCX^+ HuC-HuD^+ (**I**), PSA-$NCAM^+$ (**J**), DCX^+ $PSA\text{-}NCAM^+$ (**K**), DCX^+ CB^+ (**L**), $S100\beta^+$ (**M**), $Iba1^+$ (**N**), and phosphorylated H2AX $(\gamma H2AX)^+$ (**O**) cells. **P – Q:** Number (**P**) and orientation (**Q**) of neurites in DCX^+ HuC-HuD^+ cells. n = 14 neurologically healthy control subjects and 15 patients with BD. In **C**, Z-projection images are shown. Graphs represent mean values ± SEM. * $0.05 > p \geq 0.01$; ** $0.01 > p \geq 0.001$; *** $p < 0.001$. Detailed results of statistical comparisons are shown in **Data S1**.

Related to Figure 6.

Supplementary data. Adult hippocampal neurogenesis in patients with bipolar disorder (BD)

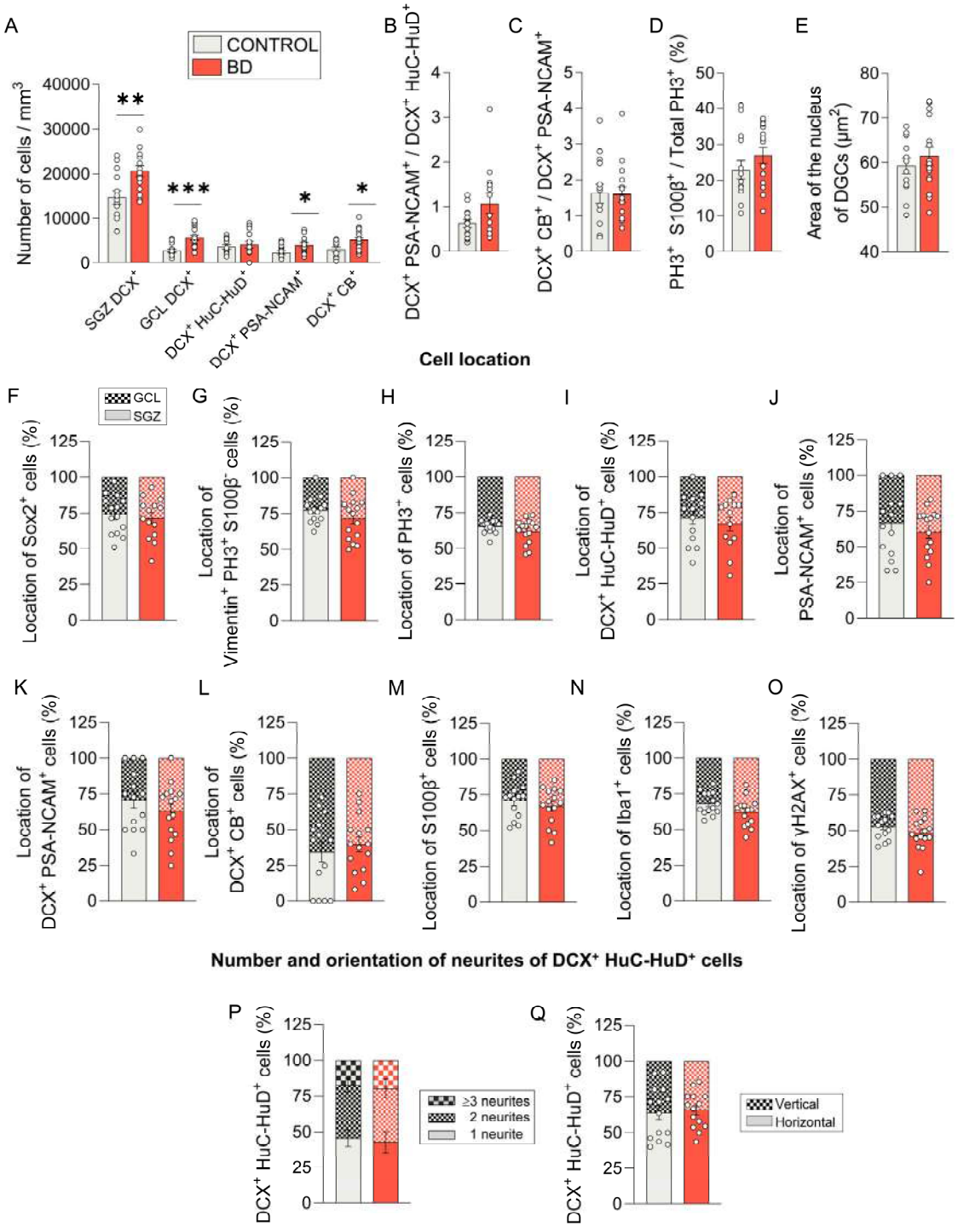

Number and orientation of neurites of DCX+ HuC-HuD+ cells

Supplementary Figure S10. Vascularization in neurologically healthy control subjects and patients with bipolar disorder (BD). A – E: Area occupied by (**A**), thickness (**B**), normalized length (**C**), and number of branches (**D**) and junctions (**E**) of *Ulex Europaeus* Agglutinin-I $(UEA1)^+$ capillaries in the subgranular zone (SGZ). **F – K:** Area occupied by (**F**), thickness (**G**), normalized length (**H**), tortuosity index (**I**), and number of branches (**J**) and junctions (**K**) of $UEA1^+$ capillaries in the granule cell layer (GCL). **L – P:** Area occupied by (**L**), thickness (**M**), normalized length (**N**), and number of branches (**O**) and junctions (**P**) of $UEA1^+$ capillaries. **Q:** Normalized ratio of the SGZ/GCL area occupied by $UEA1^+$ capillaries. n = 14 neurologically healthy control subjects and 15 patients with BD. Graphs represent mean values ± SEM. Detailed results of statistical comparisons are shown in **Data S1**.

Related to Figure 6.

Supplementary data. Dentate gyrus vascularization in neurologically healthy control subjects and patients with bipolar disorder (BD).

Vascularization in the subgranular zone (SGZ).

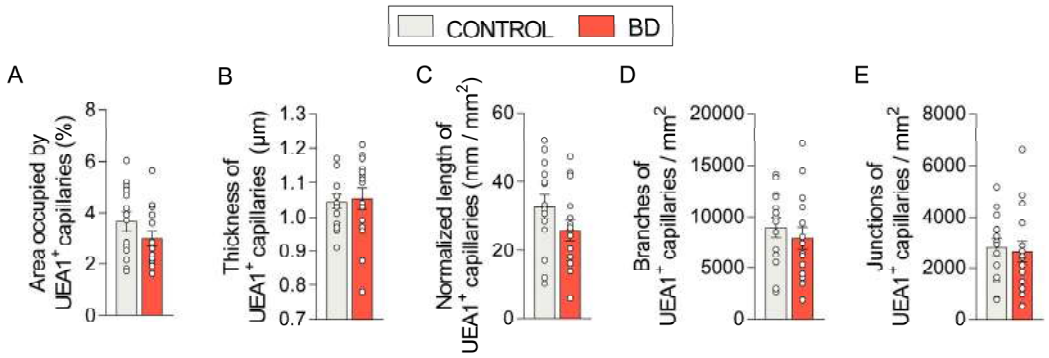

Vascularization in the granule cell layer (GCL).

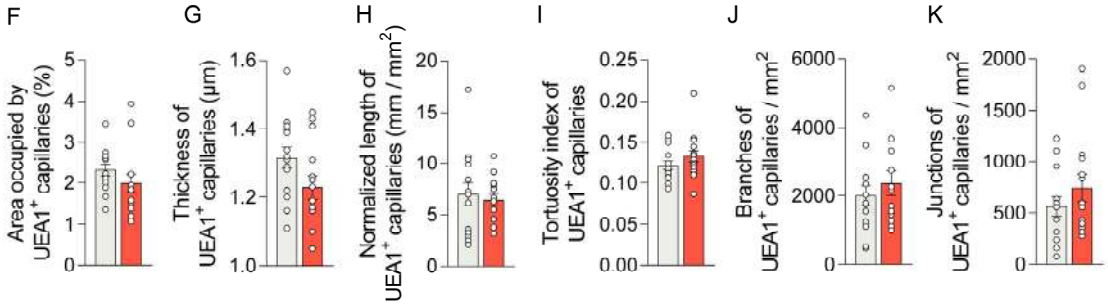

Vascularization in the dentate gyrus (SGZ+GCL).

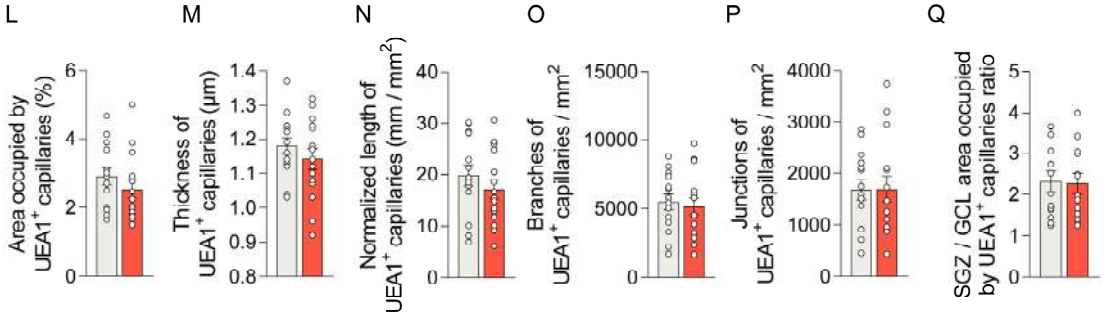

Supplementary Figure S11. Supplementary data obtained from patients with bipolar disorder (BD). A – C: Statistically significant correlations between the age of the subject and the density of doublecortin $(DCX)^+$ immature dentate granule cells (DGCs) in the subgranular zone (SGZ) (**A**), the area of the granule cell layer (GCL) occupied by *Ulex Europaeus* Agglutinin-I $(UEA1)^+$ capillaries (**B**), and the tortuosity index of SGZ $UEA1^+$ capillaries (**C**). **D – H:** Statistically significant correlations between the disease duration and the density of $Iba1^+$ cells (**D**), and the total (**E**) SGZ (**F**), and GCL (**G**) area occupied by $UEA1^+$ capillaries, and normalized length of total $UEA1^+$ capillaries (**H**). **I:** Statistically significant correlation between the onset of the disease and the tortuosity index of total $UEA1^+$ capillaries. n = 15 patients with BD. * $0.05 > p \geq 0.01$; ** $0.01 > p \geq 0.001$. Detailed results of statistical comparisons are shown in **Data S1**.

Related to Figure 6.

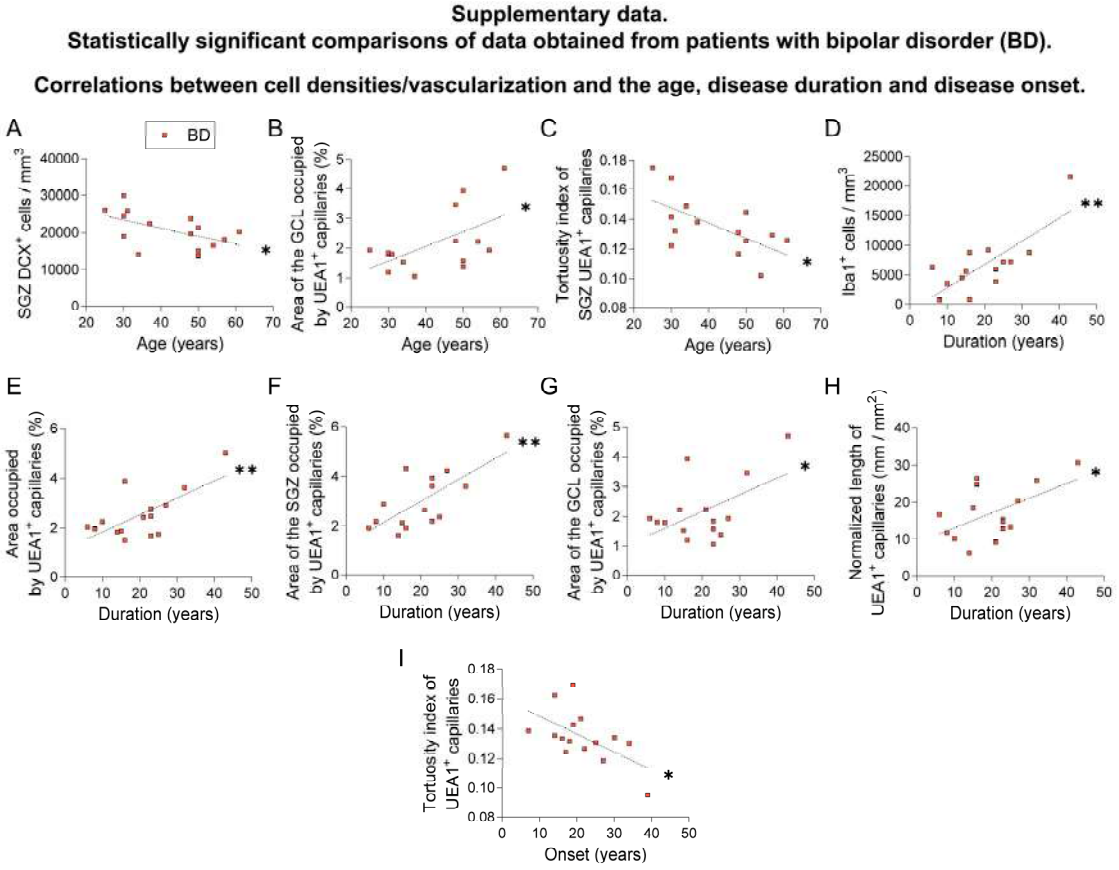

Supplementary Figure S12. Supplementary data obtained from patients with bipolar disorder (BD). A – AA: Statistically significant comparisons of data obtained from patients with BD stratified by biological sex (**A – F**), suicide (**G – J**), psychosis (**K – L**), consumption of drugs of abuse (**M – N**), treatment with anti-psychotic drugs (patients were stratified depending on whether they received a lifetime dose of fluphenazine or equivalent of more or less than 5000 mg) (**O – V**), and consumption of alcohol (**W – AA**). **A:** Location of phospho-histone 3 $(PH3)^+$ cells. **B – F:** Area of the subgranular zone (SGZ) occupied by $UEA1^+$ capillaries (**B**), normalized length (**C**) and number of branches (**D**) of SGZ $UEA1^+$ capillaries, number of junctions of total (**E**) and SGZ (**E**) $UEA1^+$ capillaries, and SGZ/ granule cell layer (GCL) $UEA1^+$ capillary thickness ratio (**F**). **G:** Density of HuC-HuD^+ cells. **H:** Percentage of DCX^+ HuC-HuD^+ out of total DCX^+ cells. **I – J:** Location of PSA-$NCAM^+$ (**I**) and DCX^+ PSA-$NCAM^+$ (**J**) immature DGCs. **K:** Percentage of DCX^+ PSA-$NCAM^+$ out of total DCX^+ immature DGCs. **L:** Location of $Iba1^+$ microglia. **M – N:** Tortuosity index of SGZ (**M**) and GCL (**N**) $UEA1^+$ capillaries. **O – Q:** Location of DCX^+ immature DGCs (**O**), thickness of total (**P**) and GCL (**Q**) $UEA1^+$ capillaries. **R – S:** Normalized length of total (**R**) and SGZ (**S**) $UEA1^+$ capillaries. **T – U:** Number of branches of total (**T**) and SGZ (**U**) $UEA1^+$ capillaries. **V:** Number of junctions of total $UEA1^+$ capillaries. **W:** Percentage of $vimentin^+$ cells that express S100β. **X:** Percentage of DCX^+ cells that express calbindin (CB). **Y – AA:** Location of $PH3^+$ (**Y**) DCX^+ PSA-$NCAM^+$ (**Z**) and PSA-$NCAM^+$ (**AA**) cells. n = 15 patients with BD. Graphs represent mean values ± SEM. * $0.05 > p \geq 0.01$; ** $0.01 > p \geq 0.001$; *** $p < 0.001$. Detailed results of statistical comparisons are shown in **Data S1**.

Related to Figure 6.

Supplementary data.
Statistically significant comparisons of data obtained from patients with bipolar disorder (BD).
Data stratified by biological sex (F: Female; M: Male).

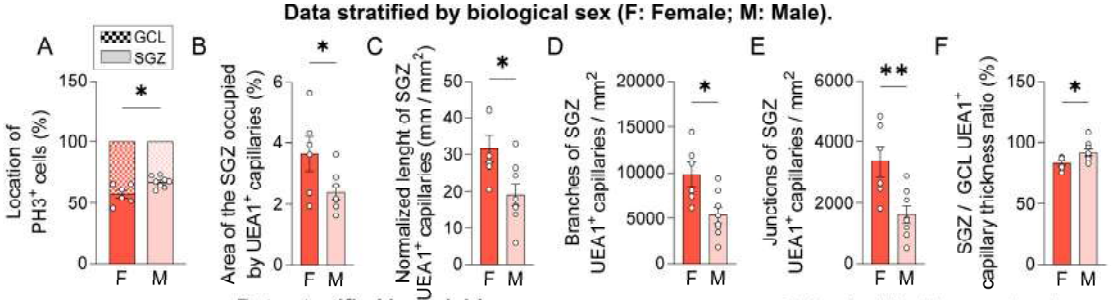

Data stratified by suicide. **Data stratified by psychosis.**

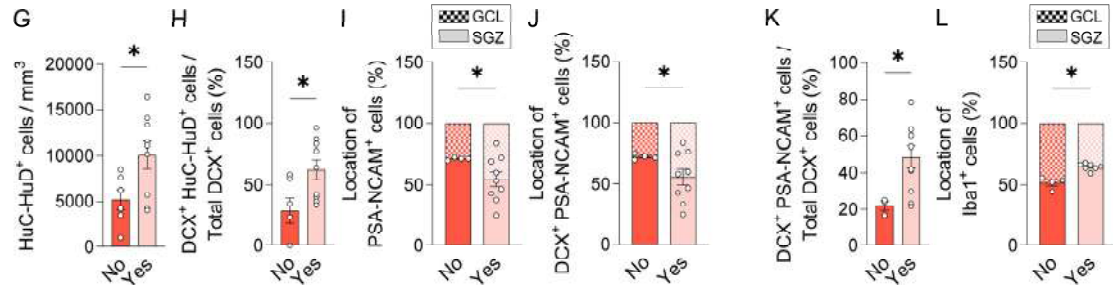

Data stratified by drugs of abuse consumption. **Data stratified by antipsychotic treatment.**

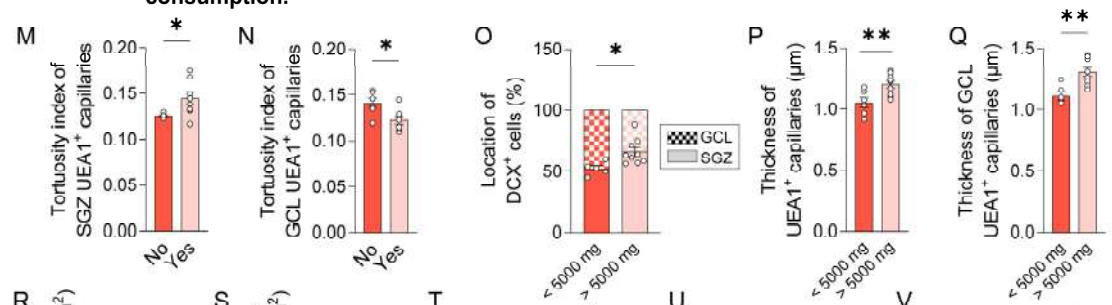

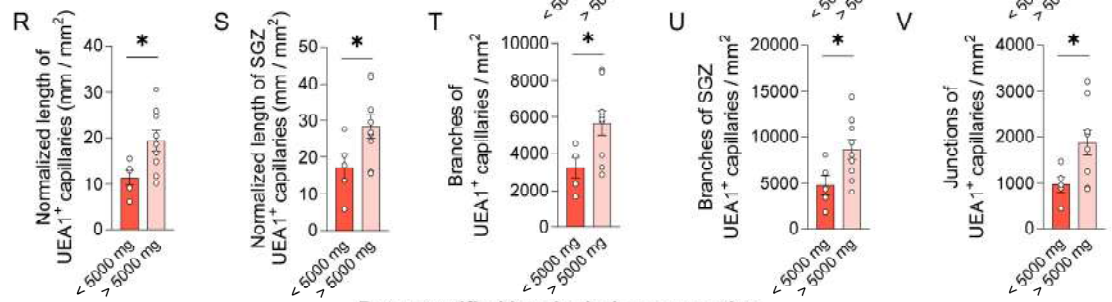

Data stratified by alcohol consumption.